Available online at www.sciencedirect.com
ScienceDirect
Lithos 97 (2007) 98–121
LITHOS
www.elsevier.com/locate/lithos

Allanite and chevkinite in A-type granites and syenites of the Graciosa Province, southern Brazil

Silvio R.F. Vlach [a,*], Guilherme A.R. Gualda [b]

[a] *Departamento de Mineralogia e Geotectônica, Instituto de Geociências, Universidade de São Paulo, Rua do Lago, 562, Cidade Universitária, 05508-080, São Paulo, SP, Brasil*

[b] *Department of the Geophysical Sciences, The University of Chicago, 5734 S. Ellis Ave., Chicago, IL 60637, USA*

Received 8 November 2005; accepted 4 December 2006
Available online 26 March 2007

Abstract

Allanite and chevkinite–perrierite are important accessory phases in the granitic and syenitic A-type rocks of the Graciosa Province, southern Brazil. Allanite–(Ce) is the main REE phase in the granites of the aluminous association – which includes metaluminous to weakly peraluminous granites – while chevkinite–(Ce) is the typical REE phase in the metaluminous syenites and alkali-feldspar syenites, and the peralkaline alkali-feldspar granites of the alkaline association.

Allanite shows complex zoning patterns but is always rich in the ferriallanite molecule and in TiO_2, a compositional trait that distinguishes allanite in A-type aluminous associations from allanite in calcic-, alkali-calcic, and calc-alkaline granitoids. Normalized REE patterns show strong fractionation of heavy over light REE, with La_N/Nd_N ratios between 3 and 5, and La_N/Y_N ratios between 200 and 400. Primary allanite is variably affected by post-magmatic transformations due to the interaction with a fluid-phase and metamictization caused by radioactive decay.

Chevkinite–(Ce) is always primary and is only present in the alkaline association. The early crystallization of chevkinite indicates that the parental magmas were probably close to REE-saturation. The REE+Y abundance in chevkinite (43–49 wt.%) is almost twice that observed in primary allanite; yet, the normalized patterns are similar in terms of fractionation between light and heavy REE, as indicated by similar La_N/Nd_N ratios in chevkinite and allanite. La_N/Y_N ratios are on average lower in chevkinite (90–300). Chevkinite compositions were altered by interaction with post–magmatic fluids, which led to marked increase in TiO_2, and a reduction in REE and Fe_T.

Post-magmatic allanite is present in both the alkaline and aluminous associations, and corresponds to ferriallanite–(Ce) in the alkaline association, and allanite–(Y) in the aluminous association. Compared to primary allanite, post-magmatic allanite–(Ce) shows smaller REE fractionation ($2<La_N/Nd_N<3$), while allanite–(Y) shows relative enrichment in the middle REE, with Sm values close to 10^5 times chondrite.

The mineralogy of the rocks indicates crystallization conditions close to the titanite–magnetite–quartz–amphibole–ilmenite (TMQAI) buffer for the aluminous association, and close to the fayalite–quartz–magnetite (FQM) buffer for the alkaline association, and temperatures between 800 and 900 °C (liquidus) and ca. 750 °C (solidus). The experimentally determined stability fields for chevkinite and allanite are in agreement with the textural evidence for early chevkinite crystallization and late allanite crystallization, even though allanite and chevkinite only rarely coexist in the alkaline association.

Wherever allanite and chevkinite coexist, they reveal reaction textures, such that it is possible that only allanite or chevkinite is stable at any given condition. The distribution of allanite and chevkinite in the alkaline association suggests that the composition of the magmas is an important control on the stability fields of these minerals, a fact that is supported by the presence of primary

* Corresponding author. Tel.: +55 11 3091 4092; fax: +55 11 3091 4258.
E-mail address: srfvlach@usp.br (S.R.F. Vlach).

0024-4937/$ - see front matter © 2006 Elsevier B.V. All rights reserved.
doi:10.1016/j.lithos.2006.12.003

allanite in rocks formed by processes of mixing and mingling of magmas. In this sense, the importance of composition on the stability of allanite and chevkinite may be larger than previously suggested.
© 2006 Elsevier B.V. All rights reserved.

Keywords: Allanite; Chevkinite; Electron probe microanalysis; A-type granites; Graciosa Province

1. Introduction

Allanite and chevkinite are important reservoirs of rare earth elements (REE) – in particular light REE – in felsic and intermediate silica-oversaturated rocks. As such, they influence significantly the behavior of these elements during magmatic differentiation and upon melting of the crust, and are of great petrologic interest. Accessory minerals like allanite and chevkinite also record important petrologic parameters, and can help elucidate magmatic processes (Wones, 1989, Robinson and Miller, 1999).

Allanite is a common accessory mineral in the vast majority of metaluminous and weakly peraluminous felsic rocks, as well as in pegmatites and hydrothermally altered rocks (cf. Gieré and Sorensen, 2004). Chevkinite and its dimorph perrierite are relatively common accessory minerals in peralkaline silica-oversaturated felsic rocks (Segalstad and Larsen, 1978; McDowell, 1979; Harding et al., 1982; Novak and Mahood, 1986; Platt et al., 1987; MacDonald et al., 2002; Troll et al., 2003). Even though there is extensive literature regarding the mineralogy and petrology of minerals of the allanite and chevkinite groups (e.g. MacDonald and Belkin, 2002, Troll et al., 2003; Gieré and Sorensen, 2004, and references therein), systematic studies of their presence and distribution in A-type rocks are scarce.

Allanite and chevkinite-perrierite are typical minerals of the granites and syenites of the Graciosa A-type Province in southern Brazil. This contribution is aimed at characterizing the distribution, compositional variations, and petrologic significance of minerals of the allanite and chevkinite groups in the Graciosa A-type Province. We use the Graciosa Province data to compare the distribution and compositions of allanite and chevkinite in A-type granites and syenites to those in other granitoid rocks and in other A-type provinces, with the goal of understanding the influence of magma composition on the stability of these minerals. The Graciosa Province is particularly well suited for a study like this as it includes granites and syenites of variable chemical affinities (i.e. metaluminous, peralkaline, weakly peraluminous), and the geology, petrography, geochemistry, and mineral chemistry of major phases have been studied in enough detail (Gualda, 2001; Garin, 2002; Garin et al., 2003; Vilalva, 2004; Vilalva and Vlach, 2006; Gualda and Vlach, in press, 2007a, 2007b).

2. The Graciosa A-type Province

2.1. Geology

The Graciosa A-type Province (Fig. 1; see also Gualda and Vlach, in press) formed in the waning stages of the Brasiliano Cycle at ca. 580 Ma (Vlach et al., 2006) and is usually considered to be a typical example of post-collisional A-type magmatism (in the sense of Liégeois, 1998; see Vlach et al., 1991; Basei et al., 1992; Siga et al., 1993; Kaul and Cordani, 2000), following the amalgamation of the Coastal Granitoid Belt to the East and the block formed by the Luiz Alves and Curitiba Microplates to the West, a collision dated at about 610–600 Ma (Siga et al., 1993).

The Graciosa Province comprises a large number of granitic and syenitic plutons, with subcircular to irregular map outlines elongated along the SSW–NNE direction, all of which were emplaced at shallow crustal levels (Hallinan et al., 1993, Gualda and Vlach, in press). The majority of the plutons crops out along the Serra do Mar Escarpment, an area characterized by extensive forest cover and rugged topography. The plutons are intrusive in Archean and Neoproterozoic rocks of the Luiz Alves and Curitiba Microplates. Bimodal volcanism is recorded in some of the plutons (e.g. Morro Redondo Pluton) as limited occurrences of basic-intermediate and silicic rocks, which may be remnants of volcanic edifices. Bimodal volcanism is also observed in contemporaneous volcano-sedimentary basins that formed prior to the inception of the Paraná Basin (Sommer et al., 2006). Dioritic rocks, mostly monzodiorites, are relatively rare in the province. Local interaction between basic-intermediate and granitic magmas gives rise to hybrid rocks of very localized occurrence.

2.2. Petrography

Like in most A-type provinces worldwide (cf. Pitcher, 1993, King et al., 1997), two main petrographic associations characterize the Graciosa Province (Vlach

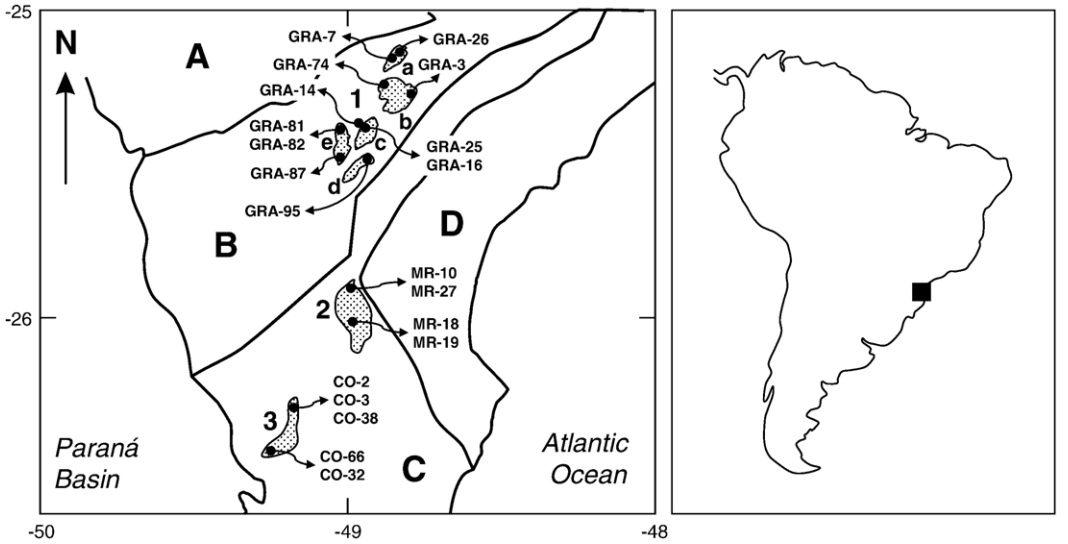

Fig. 1. Map showing the plutons of the Graciosa A-type Province (southern Brazil) included in the present study — 1: Serra da Graciosa Granites and Syenites (a — Capivari Pluton, b — Órgãos Pluton, c — Farinha Seca Pluton, d — Marumbi Pluton, e — Anhangava Pluton), 2: Morro Redondo Pluton, 3: Corupá Pluton. Location of samples used is shown approximately. The main tectonic units in southern Brazil are also indicated — A: Ribeira Fold Belt, B: Curitiba Microplate, C: Luiz Alves Microplate, D: Coastal Granitoid Belt. Adapted from Gualda and Vlach (in press).

et al., 1991, Gualda and Vlach, in press, 2007a). At one side, hypersolvus amphibole-bearing metaluminous alkali-feldspar syenites and peralkaline alkali-feldspar granites form an association of alkaline affinity. We call this the alkaline association, following Lameyre and Bowden (1982; see also Bonin et al., 1998) to emphasize the presence of both metaluminous and peralkaline varieties. In contrast, biotite-bearing metaluminous to weakly peraluminous granites and alkali-feldspar granites constitute an association of subsolvus rocks, which we refer to as an aluminous association (following Lameyre and Bowden, 1982; Vlach et al., 1990, and King et al., 1997; see, however, King et al., 2001), again to emphasize the presence of both metaluminous and peraluminous varieties. Our ongoing studies demonstrate that these two associations include several independent series, each one with particular mineralogical and petrographic variations (Gualda and Vlach, 2007a; 2007b; see also Gualda, 2001; Garin, 2002; Garin et al., 2003; Vilalva, 2004).

Rocks of the alkaline association occupy all of the Corupá and Farinha Seca Plutons, and are abundant in the Morro Redondo (northern portion), Anhangava (northern portion), and Órgãos (westernmost portion) Plutons. Rocks of the aluminous association are the only ones present in the Marumbi and Capivari Plutons, and predominate in the Morro Redondo Pluton (southern portion), Anhangava and Órgãos Plutons (Gualda and Vlach, in press).

2.2.1. Alkaline association

2.2.1.1. Corupá Pluton. The Corupá Pluton is where the alkaline association is best exposed (Garin et al., 2003). It comprises hypersolvus rocks that range from alkali-feldspar syenites and alkali-feldspar quartz syenites (predominant) to leucocratic alkali-feldspar granites. Alkali-feldspar syenites and melasyenites (M up to 65) locally form layered units of limited occurrence; in these units, rocks sometimes display subtle flow features. Textures are porphyritic or seriated, with the melasyenites and syenites being coarse-grained, and the quartz syenites and granites medium-grained; the melasyenites have cumulatic textures with alkali-feldspar as the main intercumulus phase.

The main mafic silicates in these rocks are fayalite, hedenbergite, aegirine-augite, and amphibole. The relative abundance and composition of these minerals vary with modal composition: metaluminous syenites are characterized by hedenbergite, fayalite and calcic amphibole, while the sole mafic mineral in the peralkaline granites is sodic amphibole (riebeckite). Biotite is rare and is only seen as a late-crystallizing phase in the metaluminous varieties or as the product of post-magmatic transformations.

The main accessory minerals are chevkinite, ilmenite, apatite, and zircon. Exsolved ülvospinel is observed in the more primitive syenites, while late-magmatic titanite is present in some of the quartz syenites.

Post-magmatic transformations led to the crystallization of actinolite and biotite in the syenites, and biotite, allanite, and epidote in the granites.

2.2.1.2. Morro Redondo Pluton (northern portion). The most evolved rocks within the alkaline association crop out in the northern portion of the Morro Redondo Pluton. They correspond to strongly peralkaline hypersolvus alkali-feldspar granites (Kaul and Cordani, 2000) which include rare accessory minerals typical of agpaitic rocks (Vilalva, 2004; Vilalva and Vlach, 2006).

Rocks are hololeucocratic or leucocratic and have variable texture, from porphyritic to seriated, medium to coarse-grained. Aegirine, sodic amphibole and accessory minerals fill in the interstices between the predominant mesoperthitic alkali-feldspar and quartz. Accessory minerals include astrophyllite, ilmenite, chevkinite, titanite, zircon, fluorite, narsarsukite, and britholite. The most evolved varieties are characterized by narsarsukite and other (Na, K) zirconosilicates instead of zircon. Aenigmatite is observed in some rocks with no Fe–Ti oxides. Close to the N and NW contacts of the Pluton, rocks displaying subsolidus foliation and protomylonitic texture are seen.

2.2.1.3. Anhangava, Farinha Seca, and Órgãos Plutons — Serra da Graciosa region. Rocks similar to those observed in the Corupá Pluton are found in many of the plutons of the Serra da Graciosa region. Based on modal variations, mafic mineralogy, and amphibole compositions, Gualda and Vlach (2007a) distinguish three alkaline series (1, 2 and 3), all composed by typically hypersolvus rocks. In the more evolved alkali-feldspar syenites and granites, chevkinite is the main host for light REE, and coexists with ilmenite, and occasionally titanite. Unlike in the Corupá Pluton, some of the less evolved varieties include late-magmatic allanite, ± early-magmatic chevkinite, and magnetite.

2.2.2. The aluminous association

In comparison with the alkaline association, the granites of the aluminous association are much more homogeneous in composition, and show relatively simple mineralogy, independent of their location in the province (Kaul and Cordani, 2000; Gualda and Vlach, 2007a). The most abundant rock types in the aluminous association are biotite syenogranites and monzogranites, which have porphyritic, seriated, or equigranular texture, from medium-grained to fine-grained. They are hololeucocratic or leucocratic and include plagioclase (oligoclase–andesine), perthitic alkali-feldspar, and quartz, which sometimes forms granophyric intergrowths with feldspar. Biotite and calcic amphibole (in the more mafic varieties) are the main mafic minerals. In some rocks, textures suggest the replacement of calcic amphibole by biotite, and partly corroded ilmenite is surrounded by titanite; both features can be interpreted to result from a peritectic reaction by which calcic amphibole and ilmenite are replaced by biotite, titanite, and magnetite (Speer, 1987). Allanite, titanite, magnetite, ilmenite, apatite, zircon, and fluorite complete the mineralogy and are always present in the rocks of the aluminous association.

Biotite alkali-feldspar granites are found only in the Anhangava and Marumbi Plutons. Because they correspond to the only hypersolvus biotite-bearing rocks in the province, Gualda and Vlach (2007a) group them into a separate petrographic series. They present similar textures, structure, and accessory minerals; the alkali-feldspar is mesoperthitic.

2.3. Geochemistry

From a geochemical standpoint, rocks of the Graciosa Province show many characteristics common to A-type rocks worldwide (e.g. high alkalis, FeO, Ce, Zr, Nb, etc.; see Gualda and Vlach, in press; cf. also Whalen et al., 1987, Frost et al., 2001, and references therein). With the exception of two samples from the alkaline association, which probably have some cumulatic component, all rocks fall in the field of within-plate granites (Fig. 2a) as do most A-type rocks (Frost et al., 2001). As clearly indicated by the mafic mineralogy, rocks grading from peraluminous to peralkaline are present (Fig. 2b), and metaluminous varieties are included in both petrographic associations. In these associations the metaluminous varieties correspond to the less evolved rock types, and they grade into peralkaline varieties in the alkaline association, and into peraluminous varieties in the aluminous association. These two series are also distinct in terms of the iron enrichment versus silica relations (Fig. 2c): the alkaline association shows a protracted range of SiO_2 values, and limited variation in Fe* [molecular $FeO^T/(FeO^T+MgO)$] values, while the opposite is true for the aluminous association. According to the classification of Frost et al. (2001), the alkaline association includes only ferroan varieties, while the aluminous changes from magnesian to ferroan towards the more evolved rock types. The distinction between the two associations is also evident in terms of the relative abundances of Al_2O_3 and Fe_2O_3 (Fig. 2d), with the aluminous association being enriched in Al_2O_3 over Fe_2O_3, and the reverse being true for the alkaline association. In the

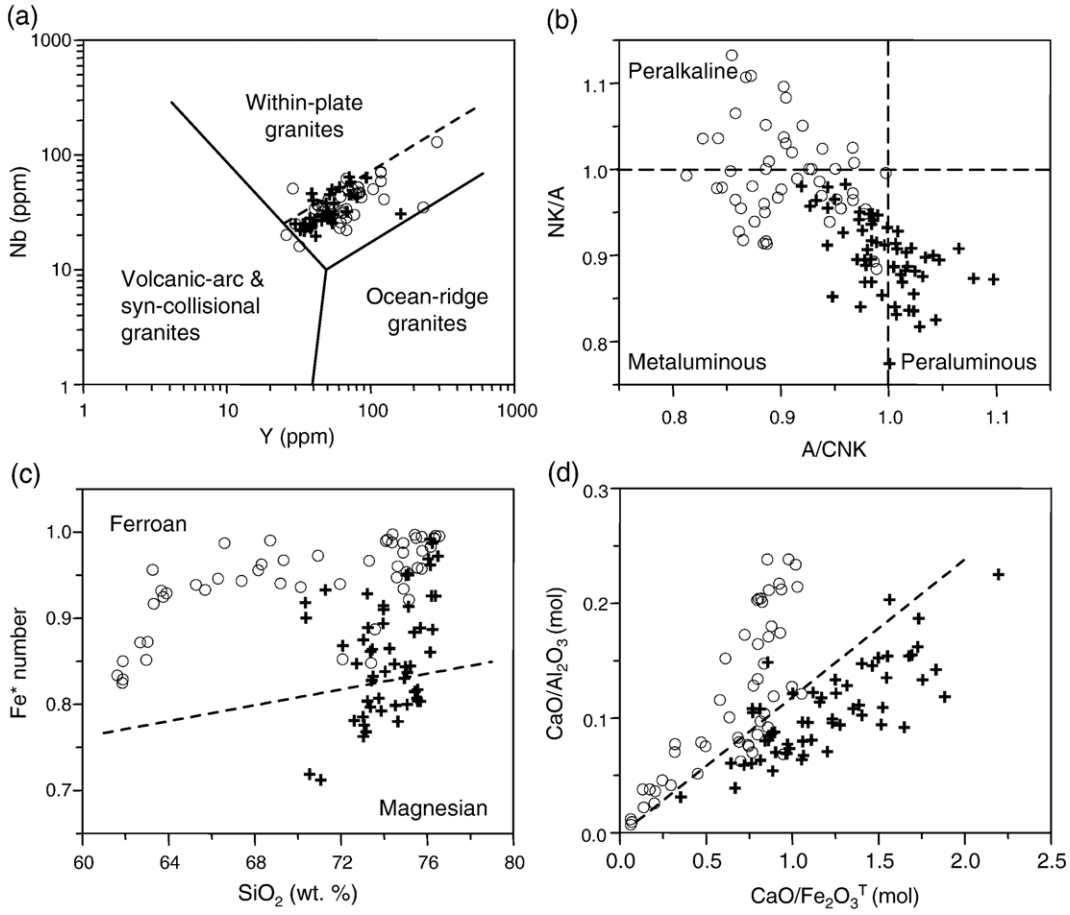

Fig. 2. Selected whole-rock chemical plots for the A-type granites and syenites of the Graciosa Province. (a) and (c) after Pearce et al. (1984) and Frost et al. (2001), respectively. Symbols: open circles, alkaline association; crosses, aluminous association. NK/A = $(Na_2O + K_2O)/Al_2O_3$ (Agpaitic Index), A/CNK = $Al_2O_3/(CaO + Na_2O + K_2O)$, and Fe* number = $FeO^T/(FeO^T + MgO)$, all quantities expressed in molecular proportions. Data sources: Kaul and Cordani (2000), Gualda and Vlach (in press) and Garin and Vlach (unpublished data). See text for discussion.

latter, the mafic mineralogy shows that the enrichment in Fe^{3+} is paralleled by enrichment in Na (Gualda and Vlach, 2007b), a feature most typical of alkaline rocks (e.g. Giret et al., 1980).

3. Sampling and methods

Representative samples from some of the most important plutons in the Graciosa Province were selected for the present study, including the main petrographic varieties of the alkaline and aluminous associations, as well as selected hybrid rocks (Fig. 1). Most samples are from plutons of the Serra da Graciosa area (Capivari, Órgãos, Farinha Seca, Marumbi, and Anhangava Plutons; cf. Gualda and Vlach, in press, 2007a). Also included are samples from the Corupá (Garin et al., 2003) and Morro Redondo (Vilalva, 2004) Plutons.

3.1. Distinction between chevkinite and perrierite

The distinction between chevkinite and perrierite can only be properly made based on the cell parameters (Haggerty and Mariano, 1983), with the β angle being close to 100° in chevkinite and 113° in perrierite. Making such a distinction is impractical for a systematic study like this, in particular considering that most crystals are partly altered and metamictic. We refined the structure of one single grain extracted from a hybrid syenite of the Farinha Seca Pluton, and obtained $\beta = 100.592 \pm 0.004$ and C2/m symmetry (unpublished data). Also, as shown below, the chemical compositions of chevkinite–perrierite from the Graciosa Province are within the compositional fields of chevkinite, as suggested by MacDonald and Belkin (2002). Accordingly, we will use the name chevkinite in the remainder of this contribution.

3.2. Analytical techniques and data treatment

Allanite and chevkinite were analyzed in C-coated polished thin sections using the JEOL JXA8600S microprobe at the Departamento de Mineralogia e Geotectônica, Instituto de Geociências, Universidade de São Paulo. Quantitative WDS analyses were performed using 20 keV, 50 nA, and 5 μm beam conditions. Back-scattered electron (BSE) images were used to qualitatively monitor compositional and textural variations.

Analyzed elements, spectral lines used for quantification, total integration times, and standards used for the WDS analyses were: Si (Kα, 20 s, olivine), Zr (Lα, 60 s, zircon), Th (Mα, 60 s, synthetic $ThSiO_4$), U (Mα, 60 s, synthetic UO_2), Ti (Kα, 20 s, titanite), Al (Kα, 20 s, synthetic YAlG), La (Lα, 20, synthetic $LaPO_4$), Ce (Lα, 20 s, synthetic $CePO_4$), Pr (Lβ, 40 s, synthetic $PrPO_4$), Nd (Lβ, 40 s, synthetic $NdPO_4$), Sm (Lβ, 60 s, synthetic $SmPO_4$), Gd (Lβ, 80 s, synthetic $GdPO_4$), Dy (Lβ, 80 s, synthetic $DyPO_4$), Er (Lα, 80 s, synthetic REE-doped glass), Yb (Lα, 80 s, synthetic $YbPO_4$), Y (Lα, 60 s, synthetic YAlG), Fe (Kα, 20 s, olivine), Mn (Kα, 40 s, olivine), Mg (Kα, 20 s, olivine), Ca, (Kα, 20 s, titanite), Sr (Lα, 60 s, synthetic $SrTiO_3$), Ba (Lα, 60 s, synthetic $BaAl_2Si_2O_8$), Na (Kα, 40 s, jadeite), K (Kα, 40 s, microcline), Nb (Lα, 60 s, metallic Nb), and Ta (Lα, 80 s, metallic Ta).

Severe interference between L lines of Eu and the lines of Nd, Pr, Dy, Fe, and Mn makes quantification of Eu impractical (cf. Exley, 1980). The abundance of F, measured and corrected for interference with Ce in selected grains, resulted close to the detection limit (ca. 0.05 wt.%). Pb abundances were always below the detection limit. Corrections for matrix-effects were calculated using the PROZA procedure (Bastin and Heijligers, 1990). Interference between the Mα lines of Th and U was corrected using a method similar to that suggested by Fialin et al. (1997). In general, detection limits are ca. 0.03–0.05 wt.% (oxide basis) for heavy elements, and ca. 0.01–0.03 wt.% for the light elements. Estimated precision is better than 2% for major elements, between 5 and 10% for minor elements, and potentially worse for trace elements.

Post-magmatic alteration and metamictization of allanite and chevkinite in old rocks may be significant. In minerals crystallized at 580 Ma, radiation damage in portions rich in Th and U is widespread, and may have facilitated subsequent chemical transformations (cf. Janeczek and Eby, 1993). Processes and products of post-magmatic alteration of allanite have already been characterized by others (e.g. Wood and Ricketts, 2000; Poitrasson, 2002), and will not be discussed here. As shown by Poitrasson (2002), significant compositional changes may take place under hydrothermal conditions even when minerals were not yet significantly affected by metamictic processes. Similar processes and transformations are likely to affect chevkinite as well, but this problem has not yet been dealt with in detail, and a brief discussion will be presented.

A total of ca. 300 analyses were obtained, but a significant fraction of these corresponds to grain portions transformed by alteration and metamictization. These portions are easily identified by the low brightness in the BSE images, low totals (down to 90 wt.%), and inadequate calculated mineral formulae. Only analyses yielding totals greater than 96.5 wt.% for allanite and 98.5 wt.% for chevkinite (all Fe as FeO) were considered, in a total of ca. 120 allanite analyses, and ca. 70 chevkinite analyses. This selection procedure inevitably introduces a bias into the results, given that analyses of portions characterized by the highest ThO_2 and UO_2 contents (1.1–2.5 and 0.1–0.5 wt.%, respectively) are systematically excluded.

Mineral formulae and cationic distributions for allanite and chevkinite were calculated following Ercit (2002) and Parodi et al. (1994), respectively. The oxidation state of Fe in allanite was evaluated using 3 procedures: (1) on the basis of 6 cations in the (T+M) positions, and considering all Mn to be in the M sites (Ercit, 2002); (2) based on the combination of the epidote–allanite and epidote–ferriallanite substitution (Petrík et al., 1995); and (3) assuming no A-site vacancies, and using the method of Droop (1987) with 8 cations and 12.5 O. The method of Ercit (2002) seems more robust and in most cases yields $Fe^{3+}/(Fe^{2+}+Fe^{3+})$ ratios intermediate between the other two methods (see further discussion below). Chevkinite analyses present a total number of negative charges close to expected (i.e., 44) for 13 cations, which suggest that almost all Fe is Fe^{2+} (MacDonald and Belkin, 2002) or that Fe^{2+} is largely predominant at least. Yang et al. (2002) report $Fe^{3+}/(Fe^{2+}+Fe^{3+})$ ratios of 0.61 in Fe-rich chevkinite–(Ce), obtained using Mössbauer spectroscopy; however their analyses yield low totals and structural OH was identified. A significant number of chevkinite analyses in the literature show some excess over the expected 13 cations, as well as Si excess in the T sites and we suspect that in part they could be indicating the presence of some Fe^{3+}. In general, a better mineral formulae was obtained using the method of Droop (1987), which yields $Fe^{3+}/(Fe^{2+}+Fe^{3+})$ ratios of 0.1–0.3, reason why this was the procedure applied (see also Jaffe et al., 1956 and MacDonald et al., 2002).

4. Results

4.1. Allanite and chevkinite texture and distribution

Many of the original textural and compositional characteristics of allanite and chevkinite crystals currently observed largely result from the overprinting by post-magmatic and metamictic transformations. It is likely that their susceptibilities to these kinds of transformations are dependent upon their primary composition and textural environment (Petrík et al., 1995; Poitrasson, 2002), such that it is possible that some of the alteration features actually emphasize original characteristics. Some typical textures of allanite and chevkinite observed in BSE images are shown in Fig. 3.

4.1.1. Allanite

Allanite crystallized in rocks of the province both as a primary magmatic phase and as a post-magmatic mineral. Primary allanite in the aluminous association is euhedral or subhedral, has variable size (0.3–3.0 mm), and shows characteristic pleochroism in shades of red or brown (Z) and of orange or reddish orange (X). Variations in pleochroism and brightness in BSE images reveal concentric, sometimes oscillatory zoning (Fig. 3a–b), as well as more irregular, patchy zoning patterns (Fig. 3c). Primary allanite includes ilmenite, magnetite, apatite, zircon, and rarely calcic amphibole, and is sometimes included in biotite, leading to the conclusion that it started crystallizing at broadly the same time as biotite, but significantly after amphibole and plagioclase.

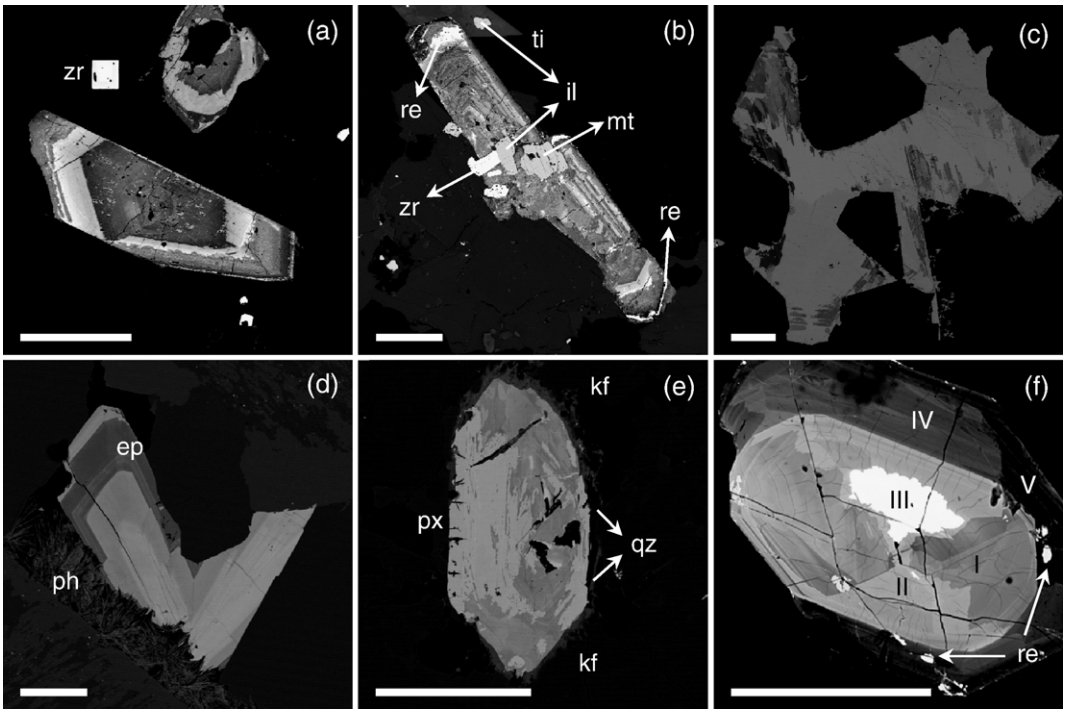

Fig. 3. BSE images showing the textures and compositional variations in allanite and chevkinite crystals of the Graciosa Province. Abbreviations — ep: epidote, il: ilmenite, mt: magnetite, ph: phyllosilicate, re: post-magmatic phases rich in REE, including fluorcarbonates, ti: titanite, zr: zircon. Bars correspond to 100 μm in all images. (a) Euhedral allanite crystals displaying oscillatory zoning; the brighter areas are characterized by high REE abundances and yield adequate mineral formulae, while the darker zones were transformed by post-magmatic fluids and subsequently by metamictization. Note the predominantly sharp contacts between the brighter intermediate zone and the outer zone (Sample GRA-26C, Capivari Pluton). (b) Euhedral allanite crystal showing fine oscillatory zoning, with inclusions of magnetite, ilmenite, and zircon. The irregular bright zones close to the rim correspond to alteration REE minerals. The crystal on the top portion corresponds to a euhedral titanite crystal with a corroded ilmenite inclusion (Sample GRA-3, Órgãos Pluton). (c) Relatively homogeneous allanite crystal interstitial to hedenbergite and calcic amphibole, showing subtle patchy zoning; the darker gray zones are variably altered (Sample GRA-81B, Anhangava Pluton). (d) Allanite within a miarolitic cavity in a peralkaline granite; darker zone in the left crystal is epidote (Sample CO-2, Corupá Pluton). (e) Euhedral chevkinite crystal with complex zoning; note the reaction rim around part of the crystal, particularly along the chevkinite–alkali–feldspar contacts (Sample MR-27, Morro Redondo Pluton). (f) Euhedral chevkinite crystal with complex zoning given by variable degrees of post-magmatic transformations; see text for detailed discussion (Sample CO-3B, Corupá Pluton).

These primary allanite crystals are variably affected by post-magmatic transformations. The darkest zones in the examples in Fig. 3a–b present lower birefringence, lighter pleochroism colors, yield low analytical totals (and particularly lower REE and Fe contents), and include aggregates of REE-rich post-magmatic phases (e.g. fluorcarbonates) and Fe oxides. All these characteristics indicate that this kind of material is strongly transformed and metamictic. In detail, the BSE images reveal some interpenetrating contacts between the brighter and the darker zones, which we interpret as replacement textures. In other samples, the darker zones developed along fractures or at the contact between allanite and other rock-forming minerals. Following Poitrasson (2002), we interpret these features as suggestive of hydrothermal alteration, later enhanced by radioactive damage and related chemical transformations.

A second generation of allanite formed under post-magmatic conditions, and is seen in sample GRA-7 (Capivari Pluton). It is characterized by anhedral interstitial crystals (0.3–0.5 mm), which are more homogeneous in composition and more pristine. They include corroded xenotime crystals, and are in close association with hydrothermal minerals (chlorite, epidote, fluorite, and Fe oxides).

Primary allanite in the alkaline association crystallized rather late, mainly as subhedral to anhedral crystals interstitial to pyroxene and amphibole (Fig. 3c), and only rarely as euhedral crystals. It is compositionally more homogeneous and may include partly corroded chevkinite crystals (see Section 5.3 below). Several crystals have abundant Fe–Ti oxide inclusions (mostly ilmenite, but also some magnetite). Hydrothermal allanite in this association is observed in the granites of the Corupá Pluton and, to a lesser extent, in the Morro Redondo Pluton. In the Corupá granites, it appears as aggregates of euhedral prisms (0.2–1.0 mm) or fibrous crystals that fill in interstices and miarolitic cavities (Fig. 3d). This kind of allanite is pristine, relatively homogeneous in composition, and is associated to epidote, Fe-rich phyllosilicates, magnetite, hematite, galena, fluorite, and fibrous zircon. Pleochroism is distinctive in shades of very dark brown or red (Z) and dark red and brown (X).

4.1.2. Chevkinite

Chevkinite is only present in the alkaline association, and is always a primary mineral. It occurs as short irregular prisms or tabular crystals (0.2–1.5 mm) that are strongly pleochroic (black to brownish-red — Z, very dark brownish-red to orange — X), and show complex internal zoning patterns. These zoning patterns mostly reflect late transformations related to hydrothermal alteration and metamictization. In the crystal shown in Fig. 3e, brighter areas in the BSE image are close to the contact with pyroxene and quartz, while the darker portions are close to the contact with alkali-feldspar. A crystal from a quartz syenite of the Corupá Pluton shows five quite distinct zones (Fig. 3f): its internal portion reveals an euhedral zone characterized by hourglass sector zoning (sectors I and II). Within sector II, an irregular patch of significantly higher brightness is seen (sector III), which has sharp lobate contacts with sector II. Surrounding this internal portion, two more zones can be seen, both of which characterized by lower average brightness in the BSE image, displaying fine oscillatory zoning, and presenting abundant inclusions of REE-rich phases irregularly distributed or along fractures. Radial fractures associated to the radioactive disintegration are clearly visible. Under the petrographic microscope, zone III is highly absorbing, while zones I and II show dark red and orange shades, and zones IV and V show orange or yellow colors; zone V is non-pleochroic and non-birefringent. WDS analyses show that only the brighter areas of the exemplified crystals display appropriate analytical totals and mineral formulae (see below).

Chevkinite started crystallizing early in the magmatic stage, giving rise to isolated euhedral crystals usually close to mafic minerals, as inclusions in calcic and sodic-calcic amphiboles (where they can be easily recognized by the presence of strong pleochroic halos), or more rarely as small inclusions in apatite, zircon, and fayalite. It is

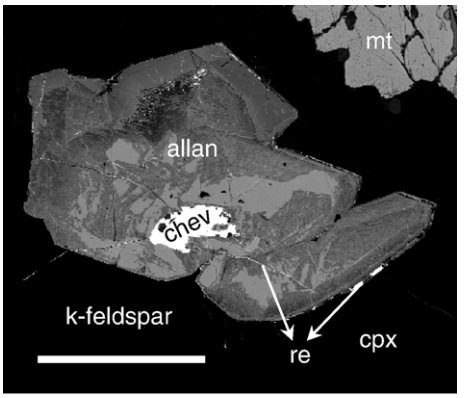

Fig. 4. BSE image showing corroded chevkinite preserved within a euhedral allanite crystal with complex patchy zoning. Darker areas observed within the allanite crystal are significantly affected by late transformations and metamictization (Sample 16A, Farinha Seca Pluton). allan: allanite; chev: chevkinite; cpx: clinopyroxene; mt: magnetite; re: REE rich late phases. Bar measures 100 μm.

Table 1
Representative electron microprobe analyses (values expressed in oxide wt.%) and mineral formulae for allanite and epidote from the Graciosa Province, southern Brazil

Pluton	Morro Redondo	Capivari		Órgãos		Farinha Seca		Anhangava		Marumbi	Corupá		
Association	alm	alm	alm	alm	alk	alk	alk	alk	alk	alk	alk	alk	alk
Sample	MR-19B	Gra-26C	Gra-7A	Gra-3B	Gra-74	Gra-16A	Gra-16B	Gra-81B	Gra-87B	Gra-95	Co-2A	Co-2A	Co-2A
Analysis	1	2	3	4	5	6	7	8	9	10	11	12	13
Point ID	2, core	4, int	1, core	7, int	6, int	1, rim(m)	3, core	6, int	3, int	2, int	2, core	4, int	3, int
SiO_2	30.01	30.22	31.90	30.44	29.67	30.48	29.96	29.52	30.26	30.51	29.85	29.99	36.53
TiO_2	1.98	2.77	0.35	2.93	3.68	2.46	2.59	4.39	3.46	2.07	1.91	5.03	0.04
Al_2O_3	11.81	11.13	16.76	10.23	8.64	11.70	10.59	7.71	9.95	11.95	8.51	9.16	19.58
FeO	15.82	17.83	13.60	17.46	19.28	16.45	17.79	19.57	18.15	15.88	20.73	17.91	15.25
MnO	0.29	0.30	1.20	0.68	0.25	0.44	0.42	0.51	0.31	0.83	0.65	0.69	0.40
MgO	1.24	0.45	0.14	0.65	0.24	0.57	0.29	0.14	0.17	0.08	bd	bd	bd
CaO	9.54	9.62	11.88	9.89	9.35	10.03	9.44	9.09	9.49	10.32	9.13	10.32	20.85
SrO	bd	bd	bd	bd	bd	bd	bd	bd	bd	bd	0.05	0.35	2.15
Na_2O	bd	0.05	bd	0.04	0.04	0.05	0.06	0.06	0.03	0.18	0.10	0.25	bd
BaO	0.04	bd	bd	0.05	0.05	bd	bd	bd	0.05	bd	bd	bd	bd
ThO_2	0.66	0.25	0.12	0.46	0.46	0.29	0.38	0.53	0.19	0.66	bd	bd	bd
UO_2	bd	bd	bd	bd	bd	bd	0.05	bd	bd	0.05	bd	bd	bd
La_2O_3	7.76	6.89	0.53	7.46	7.04	7.17	7.28	8.12	8.25	4.98	5.75	6.98	0.22
Ce_2O_3	13.04	13.25	3.74	12.77	13.11	12.83	12.95	13.32	13.16	10.05	12.80	11.28	0.34
Pr_2O_3	1.13	1.23	0.82	1.13	1.28	1.13	1.13	1.00	1.21	1.12	1.49	1.17	bd
Nd_2O_3	3.05	4.09	5.13	3.15	3.58	3.69	3.66	2.80	3.31	4.22	5.30	4.01	0.14
Sm_2O_3	0.23	0.37	2.31	0.32	0.46	0.35	0.38	0.17	0.30	0.86	0.74	0.54	bd
Gd_2O_3	0.13	0.23	2.58	0.16	0.21	0.12	0.18	0.06	0.11	0.74	0.24	0.24	0.07
Dy_2O_3	bd	0.08	1.45	0.09	0.10	bd	0.10	0.04	bd	0.26	0.10	0.07	0.12
Er_2O_3	bd	bd	0.29	bd	bd	bd	0.07	0.06	bd	bd	bd	bd	0.05
Yb_2O_3	bd	bd	0.09	bd	bd	bd	bd	bd	bd	0.11	bd	bd	bd
Y_2O_3	0.23	0.21	4.21	0.18	0.25	0.18	0.21	0.15	0.12	1.48	0.16	0.18	0.68
ZrO_2	bd	bd	bd	bd	bd	bd	bd	bd	0.05	bd	bd	bd	bd
Sum	96.94	98.94	97.10	98.09	97.68	97.93	97.54	97.24	98.57	96.35	97.50	98.15	96.42

most abundant in rocks with sodic-calcic amphiboles and is present in almost all varieties of the alkaline association, the main exception being some of the most mafic varieties in the Serra da Graciosa region, and some of the most evolved granites of the Morro Redondo Pluton.

4.1.3. Allanite and chevkinite reaction relationships

The textures observed in samples from the Serra da Graciosa with primary allanite closely associated with magnetite and chevkinite indicate that these minerals are not in equilibrium. The most typical of these textures are mantles of allanite armoring anhedral chevkinite or corroded chevkinite crystals included in euhedral to anhedral allanite (Fig. 4). In other samples chevkinite is only present as euhedral inclusions in calcic amphiboles, and allanite is the main interstitial REE-phase, forming crystals with abundant Fe–Ti oxide inclusions in their cores. Similar reaction relations were described in the Aztec Wash Pluton by Robinson and Miller (1999) and in the Shuiquangou Syenite by Jiang (2006). In the latter case, chevkinite was substituted by allanite+ilmenite in an hydrothermal environment, but in the former, as well as in the Serra da Graciosa region, the textures point clearly to a magmatic reaction launched by changes in the composition and/or intensive parameters of the crystallizing magma.

4.2. Allanite and chevkinite compositions

Allanite and other REE-rich minerals of the epidote group can be described by the general formula $A_2M_3(SiO_4)(Si_2O_7)(O,F)(OH)$, in which A=Ca, Sr, Mn^{+2}, Pb^{+2}, REE^{+3}, Th, U and M=Al, Fe^{3+}, Fe^{2+}, Mn^{3+}, Mn^{2+}, Mg, Cr^{3+},V^{3+}(Dollase, 1971, Deer et al., 1986; Gieré and Sorensen, 2004). Chevkinite and its dimorph perrierite are REE-rich titanosilicates with general formula $A_4BC_2D_2Si_4O_{22}$ in which the A position is 10 or 9-fold coordinated and is occupied by REE, Ca, Sr, Th, Na, and K. The B, C, and D positions are 6-fold coordinated and include Fe^{2+}, Mg, and Mn in B; Ti, Al,

Table 1 (*continued*)

Pluton	Morro Redondo	Capivari		Órgãos		Farinha Seca		Anhangava		Marumbi	Corupá		
Association	alm	alm	alm	alm	alk	alk	alk	alk	alk	alk	alk	alk	alk
Sample	MR-19B	Gra-26C	Gra-7A	Gra-3B	Gra-74	Gra-16A	Gra-16B	Gra-81B	Gra-87B	Gra-95	Co-2A	Co-2A	Co-2A
Analysis	1	2	3	4	5	6	7	8	9	10	11	12	13
Point ID	2, core	4, int	1, core	7, int	6, int	1, rim(m)	3, core	6, int	3, int	2, int	2, core	4, int	3, int
Formula based on 6 (M+T) cations and 12.5 O (analysis 1 to 12) and 12.5 O, all Fe as Fe^{3+} (analysis 13)													
La	0.283	0.249	0.018	0.271	0.263	0.260	0.268	0.305	0.303	0.183	0.215	0.257	0.007
Ce	0.472	0.475	0.127	0.461	0.485	0.461	0.474	0.496	0.479	0.366	0.475	0.412	0.010
Pr	0.041	0.044	0.028	0.041	0.047	0.041	0.041	0.037	0.044	0.041	0.055	0.042	0.000
Nd	0.108	0.143	0.170	0.111	0.129	0.129	0.131	0.102	0.117	0.150	0.192	0.143	0.004
Sm	0.008	0.013	0.074	0.011	0.016	0.012	0.013	0.006	0.010	0.030	0.026	0.018	0.000
Gd	0.004	0.008	0.080	0.005	0.007	0.004	0.006	0.002	0.003	0.024	0.008	0.008	0.002
Dy	0.000	0.002	0.043	0.003	0.003	0.000	0.003	0.001	0.000	0.008	0.003	0.002	0.003
Er	0.000	0.000	0.008	0.000	0.000	0.000	0.002	0.002	0.000	0.000	0.000	0.000	0.001
Yb	0.000	0.000	0.003	0.000	0.000	0.000	0.000	0.000	0.000	0.003	0.000	0.000	0.000
Y	0.012	0.011	0.208	0.010	0.013	0.009	0.011	0.008	0.007	0.078	0.009	0.009	0.030
Ca	1.010	1.010	1.184	1.045	1.014	1.056	1.011	0.992	1.011	1.101	0.991	1.103	1.842
Sr	0.000	0.000	0.000	0.000	0.000	0.000	0.000	0.000	0.000	0.000	0.003	0.020	0.103
Na	0.000	0.009	0.000	0.007	0.007	0.009	0.011	0.013	0.006	0.035	0.020	0.048	0.000
Ba	0.001	0.000	0.000	0.002	0.002	0.000	0.000	0.000	0.002	0.000	0.000	0.000	0.000
Th	0.015	0.006	0.002	0.010	0.011	0.006	0.009	0.012	0.004	0.015	0.000	0.000	0.000
U	0.000	0.000	0.000	0.000	0.000	0.000	0.001	0.000	0.000	0.001	0.000	0.000	0.000
Sum A	1.953	1.969	1.946	1.977	1.997	1.987	1.981	1.976	1.988	2.036	1.996	2.063	2.002
Fe^{3+}	0.541	0.501	0.523	0.492	0.434	0.401	0.457	0.465	0.349	0.258	0.687	0.213	1.052
Fe^{2+}	0.766	0.960	0.535	0.948	1.197	0.950	1.029	1.202	1.161	1.065	1.070	1.282	0.000
Mn	0.024	0.025	0.094	0.057	0.022	0.036	0.036	0.044	0.026	0.070	0.056	0.058	0.028
Mg	0.183	0.065	0.019	0.095	0.036	0.083	0.043	0.021	0.025	0.012	0.000	0.000	0.000
Ti	0.147	0.204	0.025	0.218	0.280	0.182	0.195	0.336	0.259	0.155	0.146	0.378	0.002
Al	1.339	1.246	1.804	1.189	1.031	1.347	1.239	0.926	1.166	1.402	1.016	1.069	1.903
Zr	0.000	0.000	0.000	0.000	0.000	0.000	0.000	0.000	0.002	0.000	0.000	0.000	0.000
Sum M	3.000	3.000	3.000	2.998	2.998	3.000	2.999	2.994	2.990	2.962	2.975	3.000	2.985
Si	2.964	2.961	2.966	3.002	3.002	2.993	2.993	3.006	3.010	3.038	3.024	2.992	3.012
Al	0.036	0.039	0.034	0.000	0.000	0.007	0.007	0.000	0.000	0.000	0.000	0.008	0.000
Sum T	3.000	3.000	3.000	3.002	3.002	3.000	3.000	3.006	3.010	3.038	3.024	3.000	3.012

Metaluminous biotite-bearing monzogranites (analyses 1 to 3), metaluminous alkali-feldspar syenites (4, 5, 9, and 10) and hybrid syenites (6, 7, and 8), peralkaline alkali-feldspar granite (11 to 13). Analysis 3 is allanite–(Y), 11, 12 and 13 are hydrothermal allanite and epidote (see Fig. 3d). alm: aluminous association, alk: alkaline association; Point ID indicates crystal number and spot location in core, intermediate (int) or rim position. (m): allanite mantles over corroded chevkinite. bd: below detection limit. K and F not detected in any of the analyses, Eu not analyzed.

Fe^{3+}, Fe^{2+}, Mg, and Mn in C; and mostly Ti in D (Gotardi, 1960; Ito, 1967; Calvo and Faggiani, 1974; MacDonald and Belkin, 2002).

Representative chemical compositions and corresponding mineral formulae of allanite and chevkinite of the Graciosa Province are presented on Tables 1 and 2 (the complete dataset can be obtained from the authors). Primary allanite in both the aluminous and alkaline associations, as well as post-magmatic allanite in the latter, is rich in the ferriallanite molecule (Kartashov et al., 2002), and correspond to ferriallanite–(Ce). Post-magmatic allanite in the aluminous association, on the other hand, is allanite–(Y). Chevkinite has chemical compositions similar to those observed for chevkinite–perrierite–(Ce) usually seen in silicic peralkaline rocks (Segalstad and Larsen, 1978; MacDonald et al., 2002; MacDonald and Belkin, 2002; Troll et al., 2003).

4.2.1. Allanite

Allanite compositions expressed in terms of total aluminum (Al^T) and REE+Y+Sr+Th are projected in the diagram of Petrík et al. (1995) shown in Fig. 5a. All allanite–(Ce) compositions plot within the allanite–ferriallanite join, which results in excellent negative

Table 2
Representative electron microprobe analyses (values expressed in oxide wt.%) and mineral formulae for chevkinite of the alkaline association from the Graciosa Province, southern Brazil

Pluton	Morro Redondo		Farinha Seca			Anhangava		Corupá					
Sample	MR-10	MR-27	Gra-14A	Gra-16A	Gra-25B	Gra-81D	Gra-87A	Co-2A	Co-3B	Co-3B	Co-3B	Co-38	Co-32D
Analysis	1	2	3	4	5	6	7	8	9	10	11	13	12
Point ID	2, core	1, core	1, int	8, int(cn)	1, core	3, core	2, rim	1, int	6, core	6, int	6, rim	4, int	2, core
SiO_2	19.30	19.14	18.96	19.98	19.78	19.64	19.68	19.20	19.76	20.54	20.47	19.53	20.10
TiO_2	18.38	18.64	14.89	19.43	18.65	18.34	18.65	18.19	19.52	25.96	28.91	18.78	19.52
Al_2O_3	0.20	0.21	0.15	0.71	0.14	0.27	0.21	0.03	0.18	0.57	0.62	0.04	0.76
FeO	10.27	10.16	12.32	9.78	11.13	10.79	10.78	11.67	10.41	8.13	7.72	10.77	9.29
MnO	0.98	0.43	0.27	0.21	0.15	0.17	0.19	0.21	0.20	0.29	0.45	0.28	0.15
MgO	bd	bd	bd	0.29	0.04	0.04	0.02	bd	0.02	0.04	0.03	bd	0.59
CaO	1.72	1.42	0.68	3.27	2.53	2.60	3.17	0.74	2.97	3.32	3.30	2.23	3.68
SrO	0.14	0.09	bd	bd	bd	bd	bd	bd	bd	0.15	0.20	bd	bd
Na_2O	bd	0.04	0.04	bd	bd	bd	0.04	0.03	bd	0.12	0.20	0.03	bd
K_2O	0.02	bd	bd	bd	bd	bd	bd	bd	bd	0.04	0.09	bd	bd
BaO	bd	bd	0.08	0.05	0.08	0.06	bd	0.05	bd	0.12	0.14	bd	0.07
ThO_2	0.15	0.14	1.06	0.39	0.72	0.38	0.49	0.21	0.26	0.44	0.68	0.45	1.05
UO_2	bd	bd	bd	bd	bd	bd	bd	bd	bd	bd	0.09	bd	bd
La_2O_3	10.14	13.24	12.06	12.13	11.25	13.75	11.98	12.65	13.44	9.96	7.88	11.09	18.77
Ce_2O_3	21.40	24.15	23.66	22.47	22.14	23.53	21.98	24.92	22.65	18.51	16.33	23.48	20.64
Pr_2O_3	2.43	2.28	2.28	2.03	2.35	2.00	2.00	2.44	2.02	1.74	1.56	2.45	1.15
Nd_2O_3	9.74	6.94	7.52	6.60	7.32	6.16	6.23	7.64	6.24	5.48	4.97	7.81	2.50
Sm_2O_3	1.57	0.70	1.16	0.58	1.05	0.69	0.81	0.89	0.55	0.55	0.53	1.04	0.14
Gd_2O_3	0.82	0.33	0.62	0.24	0.53	0.28	0.40	0.46	0.28	0.33	0.32	0.50	bd
Dy_2O_3	0.11	0.08	0.31	0.11	0.16	0.07	0.19	0.15	0.05	0.18	0.23	0.22	bd
$Er2O_3$	bd	bd	0.10	bd	bd	0.05	bd	0.07	0.05	0.10	0.10	bd	bd
Yb_2O_3	bd	bd	bd	0.04	0.07	bd	0.04	bd	0.05	0.03	0.06	bd	bd
Y_2O_3	0.46	0.13	0.61	0.40	0.68	0.37	0.55	0.26	0.37	0.53	0.69	0.44	0.06
ZrO_2	0.10	0.92	bd	0.62	0.38	0.61	0.73	0.00	0.88	0.79	0.83	0.60	0.77
Nb_2O_5	1.60	0.32	3.49	0.46	0.85	0.79	1.07	0.62	0.33	0.49	0.85	0.72	0.92
Ta_2O_5	0.05	bd	0.07	bd	bd	bd	bd	bd	bd	bd	bd	bd	bd
Sum	99.57	99.34	100.36	99.80	99.96	100.58	99.17	100.44	100.23	98.41	97.25	100.45	100.13

correlation between Al^T and Fe^T. Al^T values are in the interval 0.65–1.50 cations per formula unit (cpfu) and are larger on average for the crystals in the aluminous association (1.1–1.5 cpfu). Most post-magmatic allanite analyses and a number of analyses of primary allanite from the alkaline association plot outside the epidote–ferriallanite join. This is particularly true for allanite that coexists with chevkinite. Interestingly, some of their compositions yield REE+Y+Th+Sr larger than 1, and do not include enough Al^T to fully occupy the M(2) site. The allanite–(Y) compositions plot along the epidote–allanite join. $Fe^{3+}/(Fe^{2+}+Fe^{3+})$ ratios inferred from the diagram are mostly between 0.4 and 0.5 for primary allanite of the aluminous association, and as high as 0.5–0.6 in primary and post-magmatic allanite of the alkaline association, while allanite–(Y) has a ratio of about 0.3–0.4.

Diagrams like this are useful also to compare allanite compositions in terms of its most important end-members (Broska et al., 2000). Some caution, however, must be taken on interpretations based on the estimated $Fe^{3+}/(Fe^{2+}+Fe^{3+})$ ratios, which are dependent on the calculation procedure (cf. discussion below; see also Ercit, 2002). In Fig. 5b, we plotted about 180 compiled analyses of allanite hosted in plutonic and volcanic rocks from distinct crystallizing environments and tectonic settings elsewhere. The data reveal that allanite in igneous rocks related to extensional and/or anorogenic settings are on average enriched in the ferriallanite component, in total REE, and impoverished in Al^T when compared to allanite in calcic, alkali-calcic, and calc-alkaline rocks related to orogenic compressive regimes. The data compiled by us reinforce the findings of Broska et al. (2000) that metaluminous, magnetite-bearing rocks from active continental margins, continental volcanic arcs, and Japan-like island arcs are relatively enriched in ferriallanite and/or epidote end-members, and have higher $Fe^{3+}/(Fe^{2+}+Fe^{3+})$ ratios (between 0.35 and 0.55). In comparison, metaluminous to peraluminous,

Table 2 (*continued*)

Pluton	Morro Redondo		Farinha Seca			Anhangava		Corupá					
Sample	MR-10	MR-27	Gra-14A	Gra-16A	Gra-25B	Gra-81D	Gra-87A	Co-2A	Co-3B	Co-3B	Co-3B	Co-38	Co-32D
Analysis	1	2	3	4	5	6	7	8	9	10	11	13	12
Point ID	2, core	1, core	1, int	8, int(cn)	1, core	3, core	2, rim	1, int	6, core	6, int	6, rim	4, int	2, core
Formula based on 13 cations and 22 O													
La	0.777	1.024	0.944	0.899	0.848	1.035	0.901	0.976	1.005	0.721	0.564	0.840	1.378
Ce	1.628	1.853	1.838	1.653	1.656	1.759	1.641	1.908	1.682	1.330	1.160	1.765	1.504
Pr	0.184	0.174	0.177	0.149	0.175	0.149	0.149	0.186	0.149	0.125	0.110	0.183	0.083
Nd	0.722	0.519	0.570	0.474	0.534	0.449	0.454	0.571	0.452	0.384	0.344	0.573	0.178
Sm	0.113	0.051	0.085	0.040	0.074	0.048	0.057	0.064	0.038	0.037	0.036	0.074	0.010
Gd	0.056	0.023	0.044	0.016	0.036	0.019	0.027	0.032	0.019	0.022	0.021	0.034	0.000
Dy	0.007	0.006	0.021	0.007	0.010	0.005	0.012	0.010	0.003	0.011	0.015	0.014	0.000
Er	0.000	0.000	0.007	0.000	0.000	0.003	0.000	0.005	0.003	0.006	0.006	0.000	0.000
Yb	0.000	0.000	0.000	0.002	0.004	0.000	0.002	0.000	0.003	0.002	0.003	0.000	0.000
Y	0.051	0.014	0.069	0.042	0.073	0.040	0.059	0.029	0.040	0.055	0.071	0.048	0.006
Ca	0.382	0.318	0.155	0.704	0.553	0.568	0.691	0.166	0.646	0.699	0.686	0.490	0.784
Sr	0.017	0.011	0.000	0.000	0.000	0.000	0.000	0.000	0.000	0.018	0.022	0.000	0.000
Na	0.000	0.016	0.017	0.000	0.000	0.000	0.015	0.012	0.000	0.045	0.075	0.012	0.000
K	0.006	0.000	0.000	0.000	0.000	0.000	0.000	0.000	0.000	0.009	0.022	0.000	0.000
Ba	0.000	0.000	0.006	0.004	0.006	0.005	0.000	0.004	0.000	0.009	0.010	0.000	0.005
Th	0.007	0.006	0.051	0.018	0.033	0.018	0.023	0.010	0.012	0.020	0.030	0.021	0.048
U	0.000	0.000	0.000	0.000	0.000	0.000	0.000	0.000	0.000	0.000	0.004	0.000	0.000
Sum A	3.950	4.015	3.985	4.009	4.004	4.097	4.030	3.975	4.053	3.493	3.180	4.054	3.996
B (Fe^{2+})	1.000	1.000	1.000	1.000	1.000	1.000	1.000	1.000	1.000	1.000	1.000	1.000	1.000
Fe^{3+}	0.162	0.108	0.302	0.360	0.363	0.406	0.434	0.268	0.313	0.000	0.000	0.287	0.326
Fe^{2+}	0.623	0.674	0.886	0.284	0.539	0.435	0.405	0.775	0.452	0.335	0.253	0.563	0.219
Mn	0.172	0.076	0.049	0.035	0.026	0.030	0.033	0.037	0.035	0.048	0.074	0.049	0.025
Mg	0.000	0.000	0.000	0.087	0.012	0.011	0.005	0.000	0.007	0.011	0.008	0.000	0.176
Ti	0.872	0.939	0.377	0.937	0.865	0.815	0.860	0.862	0.976	1.831	2.218	0.900	0.923
Al	0.049	0.052	0.039	0.169	0.033	0.065	0.050	0.007	0.043	0.131	0.141	0.010	0.177
Zr	0.010	0.094	0.000	0.060	0.037	0.060	0.072	0.000	0.087	0.076	0.079	0.060	0.074
Nb	0.151	0.030	0.335	0.041	0.079	0.073	0.098	0.058	0.030	0.043	0.075	0.067	0.083
Ta	0.003	0.000	0.004	0.000	0.000	0.000	0.000	0.000	0.000	0.000	0.000	0.000	0.000
Sum C	2.041	1.972	1.991	1.974	1.953	1.895	1.957	2.008	1.942	2.476	2.848	1.935	2.004
D (Ti)	2.000	2.000	2.000	2.000	2.000	2.000	2.000	2.000	2.000	2.000	2.000	2.000	2.000
Si	4.009	4.012	4.024	4.016	4.043	4.008	4.012	4.018	4.005	4.031	3.973	4.011	4.000
Al	0.000	0.000	0.000	0.000	0.000	0.000	0.000	0.000	0.000	0.000	0.027	0.000	0.000
Sum Z	4.009	4.012	4.024	4.016	4.043	4.008	4.012	4.018	4.005	4.031	4.000	4.011	4.000

Peralkaline alkali-feldspar granites (analyses 1, 2, 3, and 8), peralkaline alkali-feldspar syenites (9 to 12), metaluminous alkali-feldspar syenites (5, 7), hybrid syenites (4, 6), and melasyenite (13). Analyses 10 and 11 are for altered chevkinite (zones II and III in Fig. 3f, respectively). Point ID indicates crystal number and spot location in core, intermediate (int) or rim position. (cn): chevkinite corroded and mantled by allanite. bd: below detection limit. F not detected in any of the analyses, Eu not analyzed.

mostly ilmenite-bearing rocks from active continental margins or collisional regimes are usually much enriched in the allanite end-member and have $Fe^{3+}/(Fe^{2+}+Fe^{3+})$ ratios between <0.35. In this latter group, a number of analyses of the La Posta Pluton and the Mecsek Mountains Granitoids are unique in that they contain a significant contribution of the clinozoisite end-member. The volcanic rocks from the Atesina Complex and some post-collisional S-/A-type granites from the Valence Mountains have somewhat higher $Fe^{3+}/(Fe^{2+}+Fe^{3+})$ ratios (0.3–0.4); these granites, classified as A-type by Broska et al. (2000), are quite distinct from the other more typical A-type rocks plotted in the diagram, showing lower values for the $Fe^{3+}/(Fe^{2+}+Fe^{3+})$ ratio as well as for the ferriallanite content. Allanite in non-alkaline rocks from extensional settings, as represented

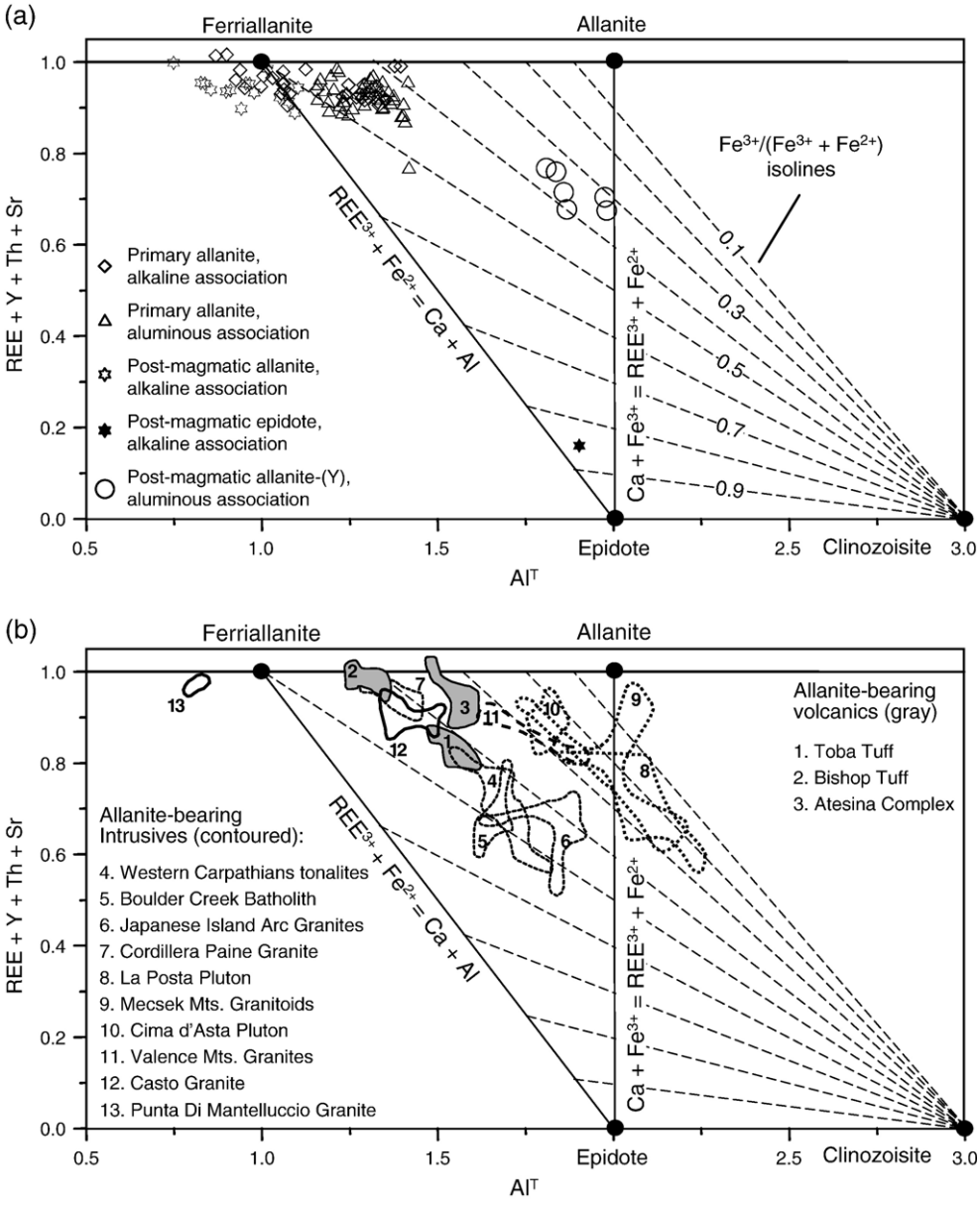

Fig. 5. (a) Compositions of allanite from the Graciosa Province plotted on the REE+Y+Sr+Th versus Al^T diagram of Petrík et al. (1995). Primary allanite: open diamonds, alkaline association; open triangles, aluminous association. Post-magmatic allanite: open stars, alkaline association; filled stars, post-magmatic epidote in alkaline association (see Fig. 3d); open circles, allanite–(Y), aluminous association. (b) Typical compositions of allanite from volcanic and intrusive rocks are plotted for comparison. References: 1: Chesner and Ettlinger (1989), 2: Hildreth (1977), 3, 8, and 10: Catlos et al. (2000), 4: Petrík et al. (1995), 5: Hickling et al. (1970), 6: Hoshino et al. (2006), 7: Michael (1984), 9 and 11: Buda and Nagy (1995), 12: Wood and Ricketts (2000), 13: Poitrasson (2002). See text for discussion.

by the Bishop Tuff and the Casto Granite show almost the same $Fe^{3+}/(Fe^{2+}+Fe^{3+})$ ratios as the metaluminous rocks from orogenic settings; their fields overlap to some extent with the Cordillera Paine Granite, which includes among the most differentiated rocks from active continental margins in our compiled data set. Some of the more allanite-rich compositions found in the Graciosa Province, in particular those from the aluminous association, overlap with those of this latter group. Allanite from alkaline rocks, as represented by the Punta di Mantelluccio Granite, show rather extreme compositions, much enriched in Fe and impoverished in Al

($Al^T < 1.0$). Several analyses for primary and post-magmatic allanite from the alkaline association in the Graciosa Province belong to this latter group.

A remarkable compositional feature of the primary and post-magmatic allanite–(Ce) from the Graciosa Province is its high TiO_2 contents (Table 1), mostly between 2 and 5 wt.% (0.10–0.38 cpfu), as illustrated in Fig. 6. This plot shows that allanite in rocks from anorogenic and/or extensional tectonic settings present distinctively higher Ti contents (ca. >0.1 cpfu) than allanite in rocks formed in compressive settings (ca. <0.1 cpfu), and among the former, allanite from alkaline series have on average higher Ti contents than allanite from the aluminous series. The excellent negative correlation between $Fe^T + Ti$ and Al^T (Fig. 7) indicates that Ti is incorporated into allanite mostly according to the coupled substitution $Ti^{4+} + Fe^{2+} = 2\ Al^{3+}$, particularly in the ferriallanite-rich varieties. This reaction is clearly favored in relatively Fe-rich and Al-poor crystallizing environments like those more typical of A-type magmas. One caveat of the diagram of Petrík et al. (1995) is that it does not take into account the effects of this substitution, such that the diagram may lead to overestimated $Fe^{3+}/(Fe^{2+} + Fe^{3+})$ ratios. This effect is not very important for Ti up to 0.15 cpfu in high-Fe allanite compositions, as is the case of several of the plotted non-alkaline rocks, but may be critical for the more Ti-rich varieties as Mantelluccio Granite and several analyses of our alkaline association. Making the proper corrections, it can be verified that the $Fe^{3+}/(Fe^{2+} + Fe^{3+})$ ratios do not depart significantly between the aluminous (0.35–0.45) and alkaline (0.35–0.50) associations, and both are close to ratios observed for the magnetite-bearing granitoids from compressive tectonic settings. It must be emphasized, however, that lower ratios may result from the calculation procedure of Ercit (2002), particularly for samples of the alkaline association (cf. Table 1).

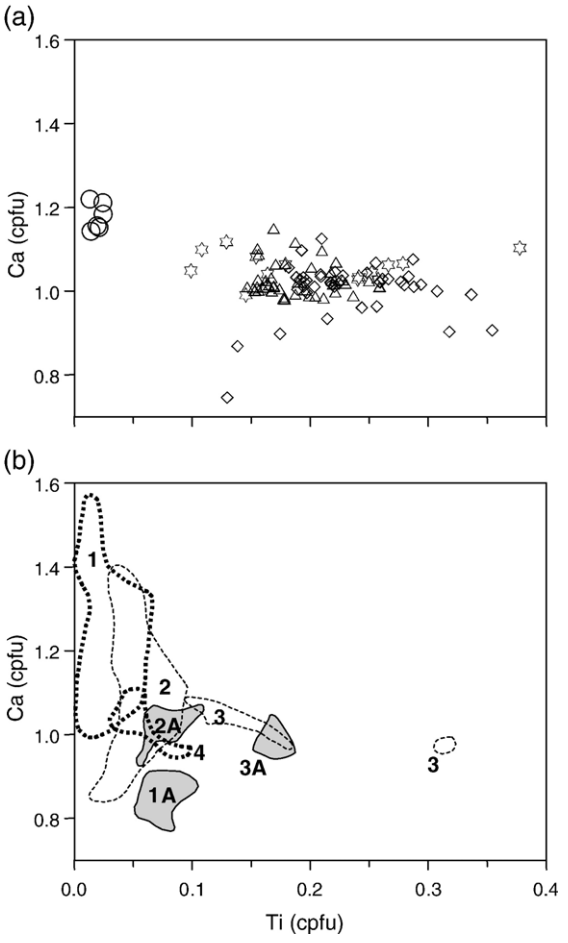

Fig. 6. Cationic Ca versus Ti plots for allanite. (a) Graciosa Province; symbols as in Fig. 5. (b) other occurrences, as plotted in Fig. 5; labeled fields are: 1: metaluminous to peraluminous, mostly ilmenite-bearing, granitoids (1A: Atesina volcanics) and 2: metaluminous, magnetite-bearing, granitoids (2A: Toba Tuff) related to compressive tectonic settings; 3: rocks related to extensional or anorogenic tectonic settings (3A: Bishop Tuff); 4: S-/A-type Valence Mts. Granites.

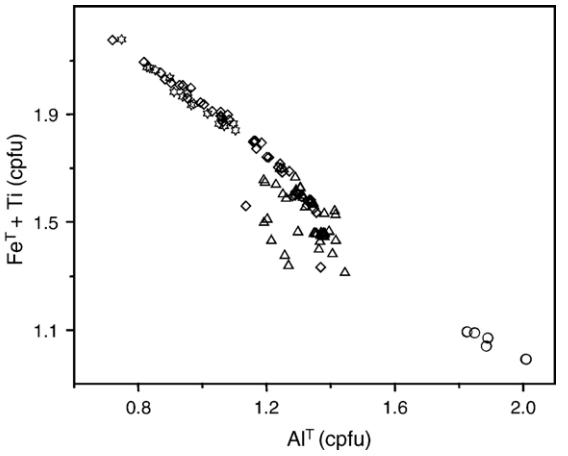

Fig. 7. Cationic $Ti + Fe^T$ versus Al^T plot for selected allanite of the Graciosa Province. Symbols as in Fig. 5. Notice the excellent correlation for crystals from the alkaline association, particularly for those rich in the ferriallanite molecule.

Allanite–(Ce) from the Graciosa Province is characterized by REE+Y abundances between 24 and 28 wt.%, while values for allanite–(Y) are close to 20 wt.%. Normalized patterns for primary allanite–(Ce) show strong fractionation of HREE over LREE (Fig. 8), with $3 < La_N/Nd_N < 5$ and $200 < La_N/Y_N < 400$. The larger variation in Gd and Dy are probably due to analytical uncertainties. One sample from the Marumbi Pluton yields less fractionated patterns, with La_N/Nd_N and La_N/Y_N values of 2 and 20, respectively. The REE patterns for primary allanite from

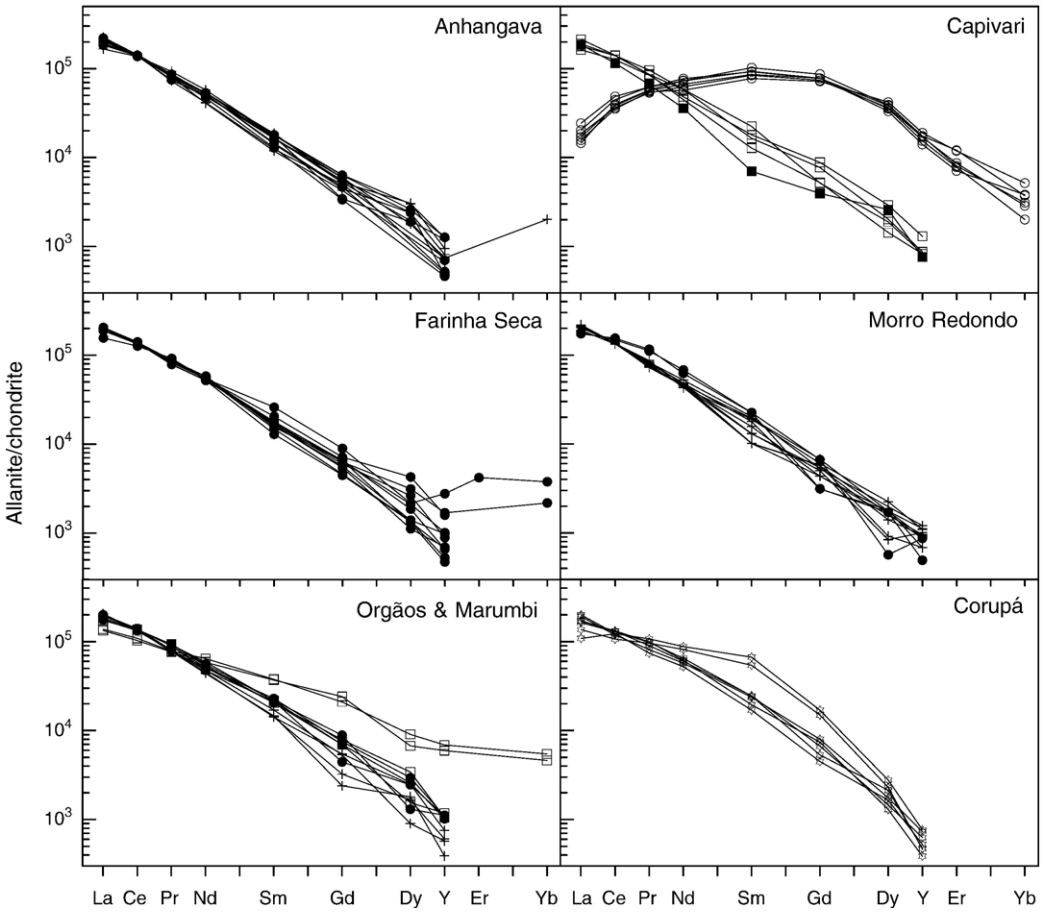

Fig. 8. Chondrite-normalized REE patterns for representative allanite of the Graciosa Province. Y is shown instead of Ho. Normalization according to Boynton (1984). Anhangava, Farinha Seca, Morro Redondo, and Órgãos Plutons: filled circles, alkaline association; crosses, aluminous association. Capivari Pluton: squares, primary allanite; circles, post-magmatic allanite.

the alkaline and aluminous associations are similar, but the La_N/Nd_N and La_N/Sm_N ratios are on average larger in the latter, in particular for the samples from the Morro Redondo and Órgãos Plutons. Fractionation is smaller in post-magmatic allanite from the alkaline association ($2<La_N/Nd_N<3$). The two analyses with the highest MREE contents correspond to the rim portion external to the epidote zone in the crystal of Fig. 3d (Table 1, analysis 13). Post-magmatic allanite–(Y) shows relative enrichment in the middle REE, with Sm values close to 10^5 times chondrite.

Among the minor elements (Table 1), MnO is in general between 0.2 and 0.9 wt.%, but reaches 1.2–1.6 in the post-magmatic allanite–(Y) and allanite–(Ce). MgO is variable, <0.2 wt.% in allanite–(Y), and as high as 1.0–1.3 in the allanite from the Morro Redondo Pluton. ThO_2 abundances are <1.80 wt.% (<1.1 in the selected analyses), and <0.2 wt.% in allanite–(Y). UO_2 is always smaller than 0.40 wt.% (<0.10 in the selected analyses).

4.2.2. Chevkinite–(Ce)

The compositions of primary chevkinite from the Graciosa Province are within the chevkinite–(Ce) field defined by MacDonald and Belkin (2002, see also Van Bergen, 1984) on the basis of FeO^T and CaO abundances (Fig. 9), even taking into account the presence of some Fe^{3+} as we evaluated. Their compositions are similar to those observed in undersaturated and oversaturared evolved rocks as compiled by MacDonald and Belkin (2002), but the Ti abundances are high on average (Fig. 10). The compositions closer to the chevkinite–perrierite boundary or within the perrierite field in Fig. 9 correspond to those with the highest Ti values, and represent crystals or crystal zones subjected to post-magmatic transformations.

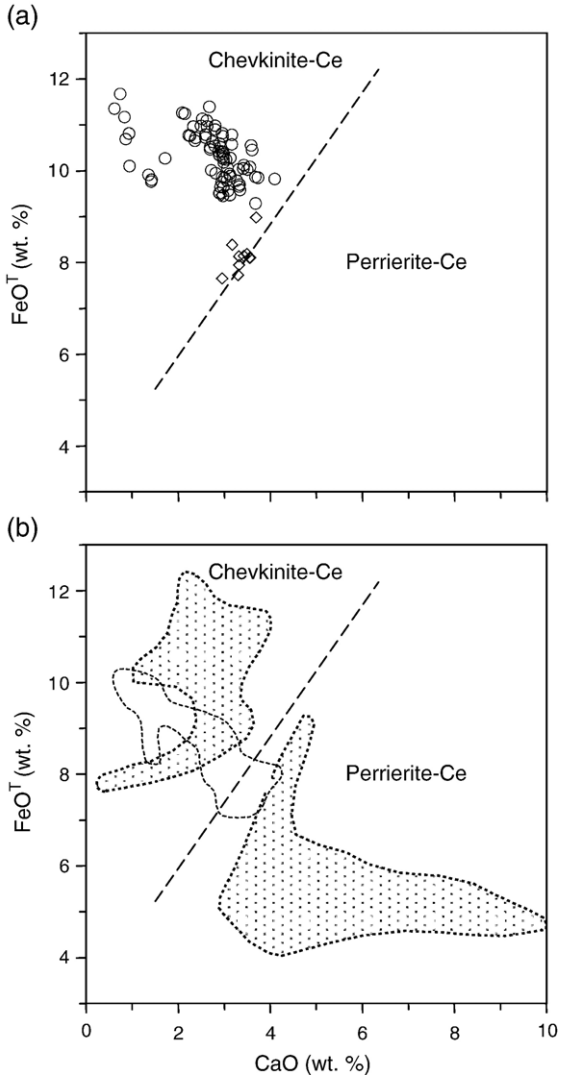

Fig. 9. (a) Chevkinite compositions of the Graciosa Province plotted on the FeO^T versus CaO diagram suggested by MacDonald and Belkin (2002) as a possible chemical discriminator between chevkinite and perrierite. Symbols: open circles, primary chevkinite; open diamonds, post-magmatic altered chevkinite. (b) Fields of normal chevkinite and perrierite mineral compositions compiled by them (shaded gray). The equation of the limit line is FeO$^T \cong 1.43$ CaO + 3.1. The light contour field corresponds to our chevkinite data, considering the estimated FeO values from microprobe data.

4.2.2.1. Primary compositional features. Compositional variations in primary chevkinite are in general limited. The tetrahedral, D, and B sites are occupied by Si, Ti, and Fe^{2+}, respectively, and the compositional variations are due to exchanges involving the A and C sites. The main substitution vectors in chevkinite–perrierite were reviewed by MacDonald and Belkin (2002), who concluded that there is no unique scheme applicable to all compositional variations observed. The main balancing reaction originally suggested by McDowell (1979), and later modified by Green and Pearson (1988) to include Sr in the A sites, is:

$$(\mathrm{Ca}+\mathrm{Sr})_\mathrm{A}+(\mathrm{Ti}^{4+})_\mathrm{C} = [(\mathrm{REE},\mathrm{Y})^{3+}]_\mathrm{A}+(\mathrm{M}^{2+,3+})_\mathrm{C} \quad (1)$$

An alternative mechanism was suggested by Parodi et al. (1994) to explain compositional variations observed in Zr-rich perrierite:

$$\mathrm{Ca}_\mathrm{A}+(\mathrm{Ti}^{4+}+\mathrm{Zr}^{4+})_\mathrm{C} = 2[(\mathrm{REE},\mathrm{Y})^{3+}]_\mathrm{A} \quad (2)$$

Della Ventura et al. (2001) showed that a combination of the balancing equations of McDowell (1979) and Parodi et al. (1994) works better to account for the compositional variations of perrierite from the Roccamonfina volcano, Italy, and suggested the reaction:

$$(\mathrm{Ca}^{2+})_\mathrm{A}+(\mathrm{Ti}^{4+})_\mathrm{C}+(\mathrm{Zr}^{4+})_\mathrm{C} = [(\mathrm{REE},\mathrm{Y})^{3+}]_\mathrm{A}+(\mathrm{M}^{2+,3+})_\mathrm{C} \quad (3)$$

The first two schemes yield good correlation to our data set, but the determination coefficient (r^2) for reaction 1 is significant larger (0.90) than for reaction 2 (0.77), as was also observed by MacDonald et al. (2002) for minerals of the chevkinite group in silicic rocks of the East African Rift. Our dataset also yields good correlation between Zr and (Ca, Sr)$_\mathrm{A}$, and good negative correlation between Zr and (REE+Y)$_\mathrm{A}$+(M$^{2+,3+}$)$_\mathrm{C}$ pointing to a balancing scheme similar to reaction (3), which gives the best correlation (r^2=0.92). Primary chevkinite from the Graciosa Province has low Sr abundances (<0.02 cpfu) and its effect on the balancing reactions cannot be well evaluated, but following Green and Pearson (1988), and taking into account some data compiled by MacDonald and Belkin (2002), we suggest that a more general equation for chevkinite–(Ce) coupled substitutions should be written as:

$$(\mathrm{Ca}+\mathrm{Sr})_\mathrm{A}+(\mathrm{Ti}^{4+}+\mathrm{Zr}^{4+})_\mathrm{C} = [(\mathrm{REE},\mathrm{Y})^{3+}]_\mathrm{A}+(\mathrm{M}^{2+,3+})_\mathrm{C} \quad (4)$$

which gives the same determination coefficient (0.92) as Eq. (3) for our dataset (Fig. 11).

The abundance of REE+Y in chevkinite from the Graciosa Province (43–49 wt.%) is almost twice that observed in primary allanite. Despite this difference in abundance, the normalized patterns reveal similar fractionation between light and heavy REE (Fig. 12).

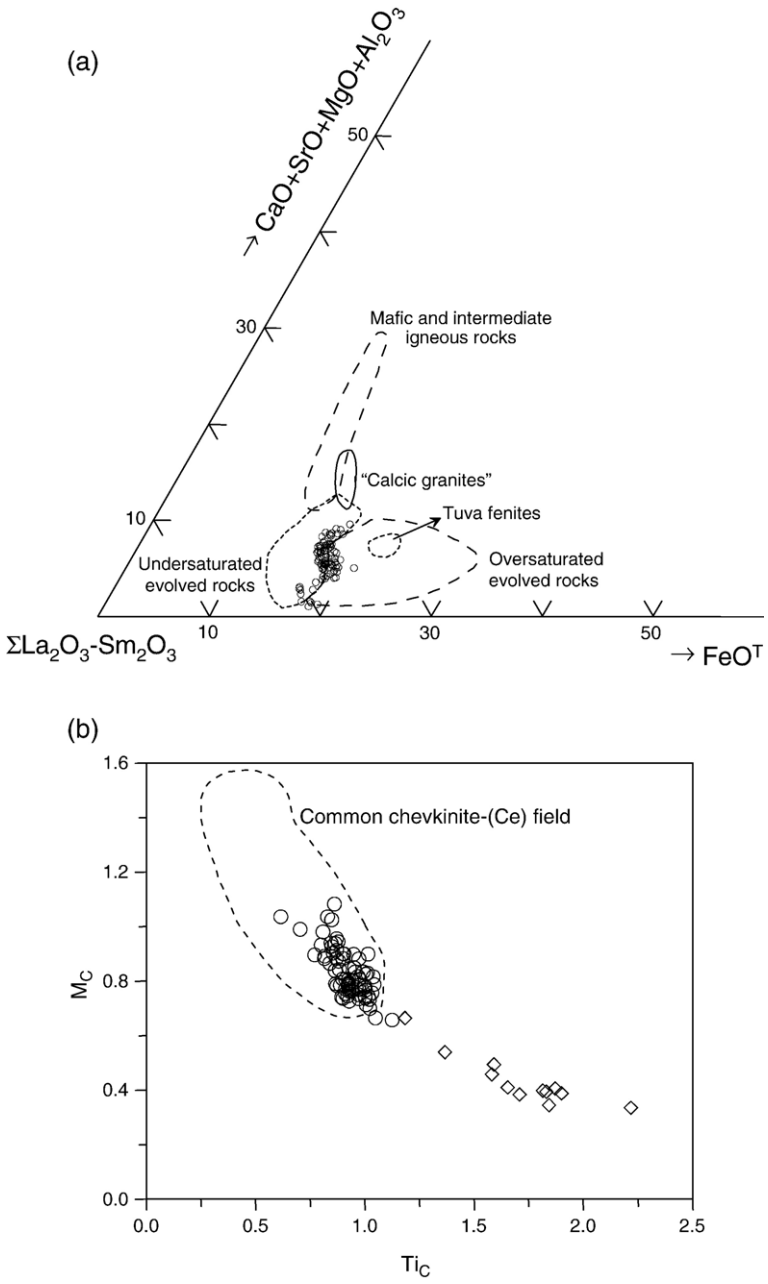

Fig. 10. (a) Chemical compositions of chevkinite of the Graciosa Province in the $\sum La_2O_3–Sm_2O_3–CaO+SrO+MgO+Al_2O_3–FeO^T$ ternary diagram of MacDonald and Belkin (2002), relating chevkinite and perrierite compositions to the host igneous rock types. Fields labeled undersaturated and saturated include only chevkinite, while the field labeled mafic and intermediate igneous rocks includes only perrierite. (b) $(M^{2+,3+})_C$ versus Ti_C cationic plot showing their inverse correlation and illustrating the relatively high Ti contents of chevkinite from the Graciosa Province as compared with occurrences elsewhere (common chevkinite–(Ce) field), compiled by MacDonald and Belkin (2002). Symbols as in Fig. 9.

Accordingly, the La_N/Nd_N ratios in chevkinite are within the same interval (3–5) or somewhat lower than those observed in allanite from the alkaline and aluminous associations, respectively (Fig. 13). La_N/Y_N ratios are on average lower than those of allanite in both associations, usually in the range 90–300. Chevkinite compositional variations in the syenites and melasyenites from the Corupá Pluton are rather limited; in the peralkaline granites of this pluton, however, LREE are significantly more abundant. The lowest HREE and Y abundances were measured in samples of the Morro Redondo Pluton, with La_N/Y_N ratios larger than 400. Where

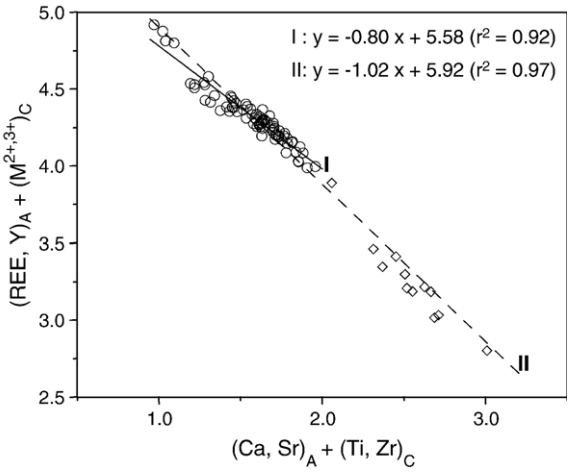

Fig. 11. Cationic plot showing compositional variations in chevkinite of the Graciosa Province according to the substitution vector represented by Eq. (4), modified from McDowell (1979), Green and Pearson (1988), and Della Ventura et al. (2001). Symbols as in Fig. 9.

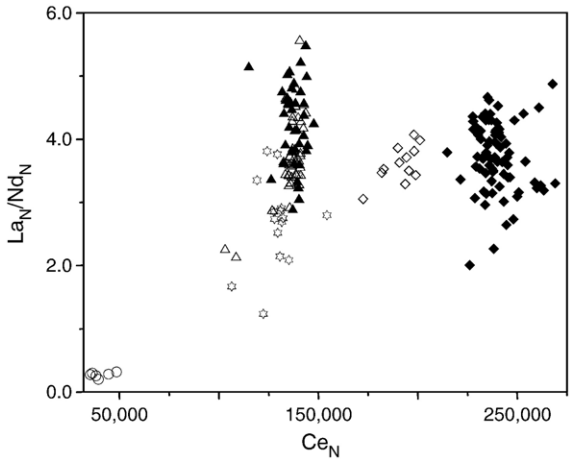

Fig. 13. La_N/Nd_N versus Ce_N plot for selected analyses of allanite and chevkinite from the Graciosa Province. Primary allanite: filled triangles, aluminous association; open triangles, alkaline association. Post magmatic allanite: stars, alkaline association; open circles, aluminous association. Primary chevkinite: filled diamonds. Post-magmatic chevkinite: open diamonds.

chevkinite does not coexist with allanite, in particular in the Farinha Seca Pluton, the normalized patterns are somewhat flatter, with higher abundances of MREE and HREE. The sample from the Marumbi Pluton that presents allanite with the least fractionated pattern (see above) contains chevkinite that also yields the least fractionated pattern in the dataset.

Minor and trace elements in chevkinite include ThO_2 (<2.50 wt.%, <1.10 wt.% in the selected analyses), UO_2 (<0.50, <0.10 in the selected analyses), MgO (<0.70), MnO (0.10–0.50), Al_2O_3 (0.05–0.80), and Nb_2O_5 (0.30–3.50). Ta_2O_5 contents are close to its detection limit (0.05–0.07). Th correlates positively with Nb and

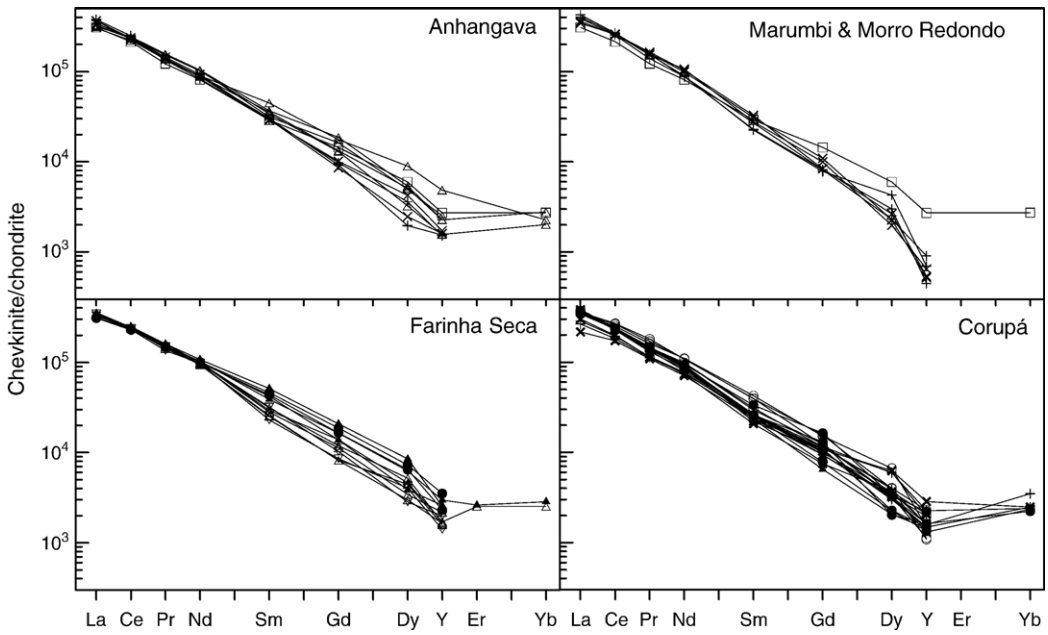

Fig. 12. Chondrite-normalized REE patterns for representative chevkinite compositions of the Graciosa Province. Y is shown instead of Ho. Normalization according to Boynton (1984). Different symbols for the same pluton represent distinct samples. Farinha Seca Pluton: filled symbols, allanite-free samples; open symbols, allanite-bearing samples. Marumbi Pluton: open squares. Corupá Pluton: open circles, alkali-feldspar granites; other symbols, syenites.

U, and negatively with Ti and (REE+Y), while Nb shows negative correlation with Ti.

4.2.2.2. Post-magmatic compositional features. Post-magmatic alteration causes important changes in the composition of chevkinite, leading to low analytical totals and poor-quality mineral formulae, with inadequate site occupancies, particularly in the C and A sites. The most important compositional variations are found in crystals or crystal zones that show textural signs of transformations as illustrated in Fig. 3. Our results indicate an increase in Ti and decrease in Fe^T, REE+Y, and analytical totals towards the darker zones in the BSE images (Table 2, analyses 9–11). It is noteworthy that even though REE amount to only 30 wt.% in the most altered zones, the fractionation patterns and La_N/Nd_N values are quite similar to those observed in primary chevkinite (Fig. 13). The relatively high fractionated pattern acquired by the hydrothermal fluids allows for the crystallization of hydrothermal ferriallanite–(Ce), as observed in the peralkaline granites of the Corupá Pluton.

When only the analyses of altered chevkinite that yield analytical totals larger than 95 wt.% are considered, it can be seen that the compositional trends are quite distinct from those observed for primary chevkinite, as exemplified by the correlations between Ti_C and Th (Fig. 14). These elements show good correlation for magmatic and post-magmatic chevkinite, but the correlation is negative and gently sloping in the former, while it is positive and more steeply sloping in the latter case. Additionally, the positive correlation between $(Ca, Sr)_A$ and $(Ti^{4+}, Zr^{4+})_C$ is poor, and Al, Na, and K are usually enriched in altered chevkinite (Table 2). The more extensively altered zones in chevkinite in general present higher Th and U, as is the case of crystal in Fig. 3e. It is important, however, that not all relatively Th-and U-rich zones display the most extensive alteration, and where the primary chevkinite crystals were armored by late allanite as seen in some hybrid rocks from the province no significant alteration is observed. In fact, the highest Th and U contents measured are for primary chevkinite compositions. Hence, these compositional changes are inferred to result from the interaction between magmatic chevkinite and hydrothermal fluids, rather than exclusively from metamictization and related transformations, as has been documented for allanite in some granitic rocks (Wood and Ricketts, 2000, Poitrasson, 2002). The compositional changes associated with alteration also result in good negative correlations between Ti_C and both Fe_T and REE, which can be very well described by the vectors in Eqs. (1)–(4). In fact, the determination coefficient for Eq. (4) considering all analyses ($r^2 = 0.97$) is significantly higher than that obtained for the primary compositions alone (Fig. 11).

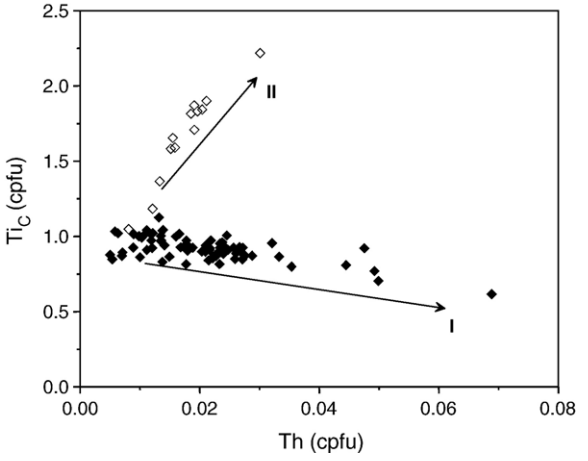

Fig. 14. Cationic Ti_C versus Th plot showing contrasted compositional trends for primary (I) and post-magmatic (II) chevkinite of the Graciosa Province. Only analyses with analytical sums larger than 95 wt.% (Fe^T as FeO) are shown.

5. Discussion

5.1. Crystallization conditions

The intensive parameters of crystallization for magmas of the Graciosa Province are not adequately constrained because conventional thermobarometers are not appropriate for many of the rock types present. Zr and P saturation temperatures (Watson and Harrison, 1983; Harrison and Watson, 1984) suggest liquidus temperatures close to 800–900 °C for samples of the alkaline and aluminous associations in the Serra da Graciosa region; however, no estimates exist for the peralkaline rocks, given that the saturation thermometers are not calibrated for such compositions (Gualda and Vlach, 2004, in press). The equilibrium between calcic amphibole and plagioclase (Holland and Blundy, 1994) yields temperatures in the interval 700–750 °C for samples of the aluminous association. Such rocks are not appropriated to evaluate crystallization pressures with the Al-in-hornblende barometer, originally proposed for calc-alkaline rocks, even considering amphibole mg# variations (Anderson and Smith, 1995; Anderson, 1996) and our results are overestimated (2–4±1 kbar), in disagreement with structural and textural evidence as well as the association with volcanic rocks that suggest emplacement pressures no greater than ca. 2 kbar (see discussion in Gualda and Vlach, in press).

Fe–Ti oxides in rocks of the province are always exsolved, particularly for the minerals of the ülvoespinel–magnetite series in the granites of the aluminous association, preventing quantitative estimations of f_{O_2} and temperature. The mafic assemblage biotite±calcic amphibole+magnetite±ilmenite+titanite of the aluminous association suggests crystallization conditions close to the titanite–magnetite–quartz–amphibole–ilmenite (TMQAI) buffer (Noyes et al., 1983, Wones, 1989), while the assemblages fayalite+hedenbergite+ülvoespinel+ilmenite±quartz observed in the more mafic syenites of the Corupá Pluton and fayalite+hedenbergite+ilmenite+quartz, characteristic of most of the alkali-feldspar syenites and granites indicates relatively more reducing conditions, close to or slightly below the fayalite–quartz–magnetite (FQM) buffer. At a reference temperature of 800 °C, the estimated difference in f_{O_2} is 2–3 log units. Compositional variations in amphiboles of the alkaline association indicate crystallization under progressively more oxidizing conditions (Gualda and Vlach, 2007b), in agreement with the late crystallization of titanite in some quartz syenites.

According to Hildreth (1979) and Chesner and Ettlinger (1989), crystallization of allanite in silica-rich magmas, as observed in the Bishop and Toba Tuffs, respectively, is limited by a critical saturation temperature, about 800 °C, under conditions above or close to the FQM buffer. Chesner and Ettlinger (1989) show that the Bishop magma crystallized in somewhat more oxidizing conditions and conclude also that high abundances of LREE are not necessary for allanite to crystallize. In experiments designed to test the stability of allanite in high-silica rhyolites, Vazquez et al. (2004) found that allanite crystallizes in the temperature interval 760–770 °C under f_{O_2} conditions close to the Ni–NiO (NNO) buffer and 7 kbar pressure. For temperatures higher than 780 °C, chevkinite is stable. They also found that the crystallization temperature of allanite is not a function of pressure, at least for pressures below 7 kbar, as indicated by a crystallization interval of 750–770 °C at 1.6 kbar pressure. In the aluminous association of the Graciosa Province, allanite textures show that it is a relatively late-crystallizing phase, and should start crystallizing at temperatures significantly below the estimated liquidus (800–900 °C), most likely when the magmas reached temperatures close to the solidus, at about 750 °C. In the more mafic syenites of the alkaline association of the province, the early crystallization of chevkinite, followed by partial substitution by allanite also agrees with the results of Vazquez et al. (2004). However, in this case, changes in magma composition may have played an important role (see Next section).

Chevkinite–(Ce) crystallizes within a wide range of temperatures and f_{O_2} values. MacDonald and Belkin (2002) revised published data based on several geothermometers and geobarometers as well as phase equilibrium diagrams and found intervals between 660–1000 °C and 1–4 kbar for temperatures and pressures, respectively, under oxygen fugacities from lower than FQM to higher than NNO (see also Novak and Mahood, 1986; Troll et al., 2003). In experiments with natural peralkaline rhyolites, and under f_{O_2} conditions of NNO−1.6 and NNO+3.6 (f_{O_2} units), Scaillet and MacDonald (2001) were able to synthesize chevkinite at 1.5 kbar pressure, temperatures between 661 and 786 °C, in relatively water-rich (2.8–5.8 wt.%) melts. They also observed that the stability field of chevkinite–perrierite grows towards higher temperatures under more oxidizing conditions and that the mimnimum temperature for water-satured melts is 660 °C. In the alkaline association of the Graciosa Province, fayalite crystallizes earlier than hedenbergite, opposite to what was observed experimentally by Scaillet and MacDonald (2001), and is only stable in the more mafic metaluminous rocks, being absent in the peralkaline types, suggesting some difference in f_{O_2} or melt compositions. Chevkinite is stable through the whole crystallization interval recorded in this association, with the exception of the most evolved peralkaline granites of the Morro Redondo Pluton. In the syenites of the Corupá Pluton, chevkinite started crystallizing close to the liquidus (possibly up to 900 °C) and under low f_{H_2O} values as indicated by the anhydrous mafic mineral assemblage, becoming more abundant in the evolved amphibole-bearing syenites. In the peralkaline granites, chevkinite probably crystallizes under conditions near water-saturation, arguably close to temperatures obtained by Scaillet and MacDonald (2001).

5.2. Chemical controls on allanite and chevkinite crystallization

With the exception of some of the more mafic syenites from the Serra da Graciosa region, allanite and chevkinite are the main LREE reservoirs in rocks of the aluminous and alkaline associations of the Graciosa Province. Chevkinite is never present in the aluminous association, even in the more mafic metaluminous rocks, which crystallized from hotter melts. Primary allanite does not crystallize in the more typical alkaline association of the Corupá Pluton, where chevkinite is ubiquitous, from the most mafic metaluminous syenites to the more evolved peralkaline granites. It becomes inevitable to conclude that these minerals may be exclusive of each association and that their crystallization is controlled by melt compositions and possibly fugacity of volatile species.

The stability of chevkinite–perrierite and allanite as a function of melt composition can be inferred from experimental data and their occurrence in igneous rocks. From the ubiquitous presence of chevkinite–perrierite in peralkaline rocks and its absence from peraluminous rocks, it can be inferred that chevkinite–perrierite is stable in peralkaline melts, but unstable in peraluminous melts. The opposite is true for allanite (e.g. Deer et al., 1986, Scaillet and MacDonald, 2001, MacDonald and Belkin, 2002, Troll et al., 2003, Gieré and Sorensen, 2004). Thus, the main question concerns the stability of allanite and chevkinite–perrierite in metaluminous melts. In the Graciosa Province, the metaluminous rocks of the alkaline association are characterized by higher NK/A and CaO/Al_2O_3, and lower A/CNK and CaO/Fe_2O_3 molecular ratios than the metaluminous varieties of the aluminous association. Compared to chevkinite, allanite has higher absolute contents of CaO and Al_2O_3, as well as higher CaO/Fe_2O_3 and significantly lower A/CNK and CaO/Al_2O_3 molecular ratios, such that it is natural to conclude that the relative abundance of Al to Ca and alkalis in the melt plays a fundamental role in the stability of allanite and chevkinite–perrierite. The typical metaluminous rocks of the alkaline association certainly were formed under relatively more reducing and anhydrous conditions than the equivalent varieties of the aluminous association, but the exact effect of the volatile species is difficult to evaluate. Both allanite and chevkinite appear to be stable in the range between above FQM to above NNO (and close to TMQAI) buffers (Chesner and Ettlinger, 1989, MacDonald and Belkin, 2002, Vazquez et al., 2004), and Scaillet and MacDonald (2001) show that chevkinite is stable close to water saturation in peralkaline melts. If melt composition is as important as our data seem to indicate, then the role of temperature on the stability of allanite and chevkinite–perrierite implied by the experiments of Vazquez et al. (2004) would probably be limited to a specific range of compositions.

5.3. Hydrothermal crystallization of allanite

Magmatic crystallization leads to a progressive increase in alkalinity, as reflected in the (Na+K)/Al ratios of amphiboles (Gualda and Vlach, 2007b) and whole-rocks of the alkaline association. It is common, however, for the post-magmatic associations to record a decrease in alkalinity, with corresponding increase in the abundance of elements like Ca and Al, as well as in the fugacity of O_2 and H_2O. This kind of evolution is widespread in the Graciosa Province, and is best displayed in quartz syenites of the Corupá Pluton, which were subjected to post-magmatic crystallization of actinolitic amphibole and biotite, probably simultaneous to the alteration of primary chevkinite. In the most evolved peralkaline granites, the post-magmatic enrichment of Ca and Al was sufficient for ferri-allanite and epidote to crystallize with biotite during the hydrothermal stage, indicating that the evolution of magmas of alkaline affinity in plutonic conditions can lead to residual fluids with adequate composition for allanite to crystallize. Jiang (2006) attributed, however, the hydrothermal substitution of chevkinite for allanite in the Shuiquangou syenitic intrusion to an external fluid which has supplied Al and Ca, among other elements. Comparing the compositions of the hydrothermal allanite crystallized in the alkaline and aluminous association, particularly for the Corupá and Capivari Plutons, contrasted hydrothermal fluid signature may be inferred, those associated with the alkaline rocks being richer in LREE while those associated with the aluminous association being M-HREE richer.

5.4. The substitution of chevkinite for allanite in hybrid rocks

The late crystallization of allanite, usually substituting chevkinite, in some of the most mafic rocks of the alkaline association in Serra da Graciosa region, is in principle compatible with the interpretations of Robinson and Miller (1999) and the experiments of Vazquez et al. (2004) that suggest crystallization of chevkinite at higher temperatures, followed by crystallization of allanite at lower temperatures. However, it must be emphasized that allanite (+magnetite) is only present in the more mafic rocks and is completely lacking in the more evolved varieties – which become gradually more peralkaline (or even agpaitic) – where chevkinite and ilmenite are common accessory phases (Gualda and Vlach, 2007a). Furthermore, in the alkaline association of the Corupá Pluton, primary allanite is never present, and chevkinite is stable in all rocks studied, from the most mafic metaluminous melasyenites (some of which contain exsolved ülvospinel) to the most evolved peralkaline granites. In both cases, the effect of temperature seems to have been limited when compared to that of melt composition.

In the Graciosa Province in general, rocks in which chevkinite appears substituted by allanite crop out in areas where field evidence indicates mingling and local mixing between syenitic and dioritic melts. The most typical hybrid syenites contain centimeter- to decimeter-sized microgranular enclaves, with dioritic or monzodioritic compositions, as well as millimeter-sized mafic clots,

composed mainly of clinopyroxene, hornblende, and Fe–Ti oxides. In some cases, late-magmatic oligoclase and biotite are seen in millimeter-size zones adjacent to the contacts between syenites and dioritic enclaves. These features clearly indicate that the syenitic melts incorporated variable fractions of dioritic melts in the magmatic stage. We argue that the mixing significantly changes the melt composition, causing the destabilization of chevkinite and its partial or complete substitution by allanite and Fe–Ti oxides (mainly ilmenite), and possibly giving rise to an increase in fO_2 as suggested by the relative abundance of magnetite in these rocks, a theme to be explored in a future contribution (Vlach and Gualda, in preparation). We also speculate that mixing may be widespread in relatively mafic rocks of the alkaline association that include allanite+magnetite – even with no chevkinite – and this could explain the high Ti abundance in allanite from these rocks, as well as for the abundant ilmenite inclusions found in several allanite crystals.

6. Summary and conclusions

Allanite–(Ce) and chevkinite–(Ce) are the main primary repositories for REE – in particular light REE – in the granitic and syenitic A-type rocks of the Graciosa Province, southern Brazil. Allanite is the main REE phase in the metaluminous and peraluminous granites of the aluminous association, while chevkinite is typical in the metaluminous and peralkaline syenites and alkali-feldspar granites of the alkaline association.

The composition of allanite in granitoid and syenitic rocks is closely related to the original melt compositions and the crystallization environment. Allanite in the Graciosa Province and in several A-type rocks related to extensional or anorogenic tectonic regimes elsewhere is characteristically richer in the ferriallanite molecule, in REE, and in TiO_2, and poorer in Al_2O_3 than allanite in calcic, calc-alkaline or alkali-calcic associations related to compressive tectonics. The TiO_2 abundances of the former are 2- to 5-fold greater than in other granitoid rocks. Among the A-type rocks, allanite in the typical alkaline types shows the highest TiO_2 and FeO^T and lowest Al_2O_3 contents. The estimated $Fe^{3+}/(Fe^{2+}+Fe^{3+})$ ratios in allanite of the aluminous and alkaline associations are between 0.35 and 0.50, quite similar to those observed in relatively oxidized calc-alkaline granitoids. Both the alkaline and the aluminous associations of the Graciosa Province include allanite crystallized in a post-magmatic, hydrothermal stage, but a relatively Ti-rich and Al-poor ferriallanite is observed in the former, while an Al-rich, low $Fe^{3+}/(Fe^{2+}+Fe^{3+})$ allanite–(Y) is seen in the latter.

Chevkinite–(Ce) is always primary and is only present in the alkaline association. Its early crystallization suggests that the parental magmas were close to REE-saturated. Compositions observed in the Graciosa Province are similar to, but on average richer in Ti than those seen in chevkinite–(Ce) from evolved undersaturated and saturated rocks of alkaline affinity worldwide. Reaction between chevkinite and late hydrothermal fluids leads to significant post-magmatic alteration, characterized by a crystallochemically-controlled reduction in REE and Fe^T, and increase in Ti abundances.

Melt composition, in particular the relative abundances of alkalis, Ca, and Al, played a fundamental role on the stability of allanite and chevkinite in the A-type rocks of the Graciosa Province. In contrast, temperature seems to be of secondary importance, and possibly limited to a specific range of melt compositions. The inferred crystallization conditions of the aluminous and alkaline associations are close to the TMQAI and FQM buffers, respectively, but it appears that the f_{O_2} was not a fundamental parameter controlling the crystallization of allanite and chevkinite in each association. Wherever allanite and chevkinite occur together, the textures indicate that allanite is of late crystallization and partially substitutes chevkinite; these rocks show several features indicative of a hybrid origin, related to mingling and partial mixing between syenitic and dioritic melts.

Acknowledgements

We are indebted to Ian Steele for the structural refinement of a chevkinite crystal. We would like to acknowledge the continued support by FAPESP (Fundação de Amparo à Pesquisa do Estado de São Paulo) to the Laboratório de Microssonda Eletrônica, Departamento de Mineralogia e Petrologia, Universidade de São Paulo. Suggestions and comments by two anonymous reviewers and editorial handling by Carol D. Frost helped improved the original manuscript and are much appreciated.

References

Anderson, J.L., 1996. Status of thermobarometry in granitic batholiths. Transactions of the Royal Society of Edinburgh: Earth Sciences 87, 125–138.

Anderson, J.L., Smith, D.R., 1995. The effect of temperature and oxygen fugacity on Al-in-hornblende barometry. American Mineralogist 80, 549–559.

Basei, M.A.S., Siga Jr., O., Machiavelli, A., Mancini, F., 1992. Evolução tectônica dos terrenos entre os Cinturões Ribeira e Dom Feliciano (PR-SC). Revista Brasileira de Geociências 22, 216–221.

Bastin, G.F., Heijligers, H.J.M., 1990. Progress in electron-probe microanalysis. Materialwissenschaft und Werkstofftechnik 21, 90–92.

Bonin, B., Azzouni-Sekkal, A., Bussy, F., Ferrag, S., 1998. Alkali-calcic and alkaline postorogenic (PO) granite magmatism: petrologic constraints and geodynamic settings. Lithos 45, 45–70.

Boynton, W.V., 1984. Cosmochemistry of the rare earth elements: meteorite studies. In: Henderson, P. (Ed.), Rare earth element geochemistry. Elsevier, Amsterdan, pp. 63–114.

Broska, I., Petrík, I., Williams, T.C., 2000. Coexisting monazite and allanite in peraluminous granitoids of the Tribeè Mountains, Western Carpathians. American Mineralogist 85, 22–32.

Buda, G., Nagy, G., 1995. Some REE-bearing accessory minerals in two types of Variscan granitoids, Hungary. Geologica Carpathica 46, 67–78.

Calvo, C., Faggiani, R., 1974. A re-investigation of the crystal structures of chevkinite and perrierite. American Mineralogist 59, 1277–1285.

Catlos, E.J., Sorensen, S.S., Harrison, T.M., 2000. Th–Pb ion-microprobe dating of allanite. American Mineralogist 85, 633–648.

Chesner, C.A., Ettlinger, A.D., 1989. Composition of volcanic allanite from the Toba Tuffs, Sumatra, Indonésia. American Mineralogist 74, 750–758.

Deer, W.A., Howie, R.A., Zussman, J., 1986. Rock-Forming Minerals. 1B. Disilicates and Ring Silicates, 2nd ed. Longman Scientific and Technical, London. 629 pp.

Della Ventura, G., Williams, C.T., Raudsepp, M., Bellatreccia, F., Caprilli, E., Giordano, G., 2001. Perrierite–(Ce) and zirconolite from syenitic ejectum of the Roccamonfina volcano (Latium, Italy): implications for the mobility of Zr, Ti, and REE in volcanic environments. Neues Jahrbuch für Mineralogie Monatshefte 385–402.

Dollase, W., 1971. Refinement of the crystal structures of epidote, allanite, and hancockite. American Mineralogist 56, 447–464.

Droop, G.T.R., 1987. A general equation for estimating Fe^{3+} in ferromagnesian silicates and oxides from microprobe analysis, using stoichiometric criteria. Mineralogical Magazine 51, 431–437.

Ercit, T.S., 2002. The mess that is "allanite". Canadian Mineralogist 40, 1411–1419.

Exley, R.A., 1980. Microprobe studies of REE-rich accessory minerals: implications for Skye granite petrogenesis and REE mobilty in hydrothermal systems. Earth and Planetary Science Letters 48, 97–110.

Fialin, M., Outrequin, M., Staub, P.F., 1997. A new tool to treat peak overlaps in electron-probe microanalysis of rare-earth element L-series X-ray. European Journal of Mineralogy 9, 965–968.

Frost, B.R., Barnes, C.G., Collins, W.J., Arculus, R.J., Ellis, D.J., Frost, C.D., 2001. A geochemical classification for granitic rocks. Journal of Petrology 42, 2033–2048.

Garin, Y., 2002. Mineralogia e petrologia da associação alcalina de sienitos e granitos de Tipo-A do Maciço Corupá (SC). Unpublished M.Sc. thesis, Universidade de São Paulo, 168 pp.

Garin, Y., Vlach, S.R.F., Tassinari, C.C.G., 2003. Sr and Nd isotope signatures of A-type alkaline syenites, granites, and associated diorites and hybrid rocks from the Corupá Massif (SC), Serra do Mar Province, S Brazil. 4th South American Symposium on Isotope Geology. Salvador, Brazil. Short Papers, vol. 2, pp. 556–559.

Gieré, R., Sorensen, S.S., 2004. Allanite and other REE-rich epidote-group minerals. In: Liebscher, A., Franz, G. (Eds.), Epidotes. Reviews in Mineralogy and Geochemisty, vol. 56, pp. 431–493.

Giret, A., Bonin, B., Leger, J.-M., 1980. Amhibole compositional trends in oversaturated and undersaturated alkaline plutonic ring-complexes. Canadian Mineralogist 18, 481–495.

Gotardi, G., 1960. The crystal structure of perrierite. American Mineralogist 45, 1–14.

Green, T.H., Pearson, N.J., 1988. Experimental crystallization of chevkinite/perrierite from REE-enriched silicate liquids at high pressure and temperature. Mineralogical Magazine 52, 113–120.

Gualda, G.A.R., 2001. Evolução petrográfica e mineralógica das associações alcalina e aluminosa dos Granitos Tipo-A da Graciosa, PR. Unpublished M.Sc. thesis, Universidade de São Paulo, 250 pp.

Gualda, G.A.R., Vlach, S.R.F., 2004. Petrographic and mineralogical evolution of the alkaline and aluminous associations of the Graciosa A-type granites, Brazil. Geochimica et Cosmochimica Acta 68, A675.

Gualda, G.A.R., Vlach, S.R.F., 2007a. The Serra da Graciosa A-type Granites and Syenites, southern Brazil. Part 2: Petrographic and mineralogical evolution of the alkaline and aluminous associations. Lithos 93, 310–327.

Gualda, G.A.R., Vlach, S.R.F., 2007b. The Serra da Graciosa A-type Granites and Syenites, southern Brazil. Part 3: Magmatic evolution and post-magmatic breakdown of amphiboles of the alkaline association. Lithos 93, 328–339.

Gualda, G.A.R., Vlach, S.R.F., in press. The Serra da Graciosa A-type granites and syenites, southern Brazil. Part 1: Regional setting and geological characterization. Anais da Academia Brasileira de Ciências.

Haggerty, S.E., Mariano, A.N., 1983. Strontian-loparite and strontio-chevkinite: two new minerals in rheomorphic fenites from the Paraná Basin carbonatites, South America. Contributions to Mineralogy and Petrology 84, 365–381.

Hallinan, S.E., Mantovani, M.S.M., Shukowsky, W., Braggion Jr., I., 1993. Estrutura do escudo Sul-Brasileiro: Uma revisão através de dados gravimétricos e magnetométricos. Revista Brasileira de Geociências 23, 201–214.

Harding, R.R., Merriman, R.J., Nancarrow, P.H.A., 1982. A note on the occurrence of chevkinite, allanite, and zirkelite on St. Kilda, Scotland. Mineralogical Magazine 46, 445–448.

Harrison, T.M., Watson, E.B., 1984. The behavior of apatite during crustal anatexis — equilibrium and kinetic considerations. Geochimica et Cosmochimica Acta 48, 1467–1477.

Hickling, N.L., Phair, G., Moore, R., Rose Jr., H.J., 1970. Boulder Creek Batholith, Colorado. Part I: allanite and its bearing upon age patterns. Geological Society of America Bulletin 81, 1973–1994.

Hildreth, E.W., 1977. The magma chamber of the Bishop Tuff: Gradients in temperature, pressure, and composition. Ph.D. thesis, University of California, Berkeley, California, 328 pp.

Hildreth, E.W., 1979. The Bishop Tuff: evidence for the origin of compositional zonation in silicic magma chambers. Geological Society of America Special Paper 180, 43–75.

Holland, Y., Blundy, J., 1994. Non-ideal interactions in calcic-amphiboles and their bearing on amphibole-plagioclase thermometry. Contributions to Mineralogy and Petrology 116, 433–447.

Hoshino, M., Kimata, M., Shimizu, M., Nishida, N., Fujiwara, T., 2006. Allanite–(Ce) in granitic rocks from Japan: genetic implications of patterns of REE and Mn enrichment. Canadian Mineralogist 44, 45–62.

Ito, J., 1967. A study of chevkinite and perrierite. American Mineralogist 52, 1094–1104.

Jaffe, H.W., Evans Jr., H.T., Chapman, R.W., 1956. Occurrence and age of chevkinite from de Devil's Slide fayalite–quartz syenite near Stark, New Hampshire. American Mineralogist 41, 474–487.

Janeczek, J., Eby, R.K., 1993. Annealing of radiation damage in allanite and gadolinite. Physics and Chemistry of Minerals 19, 343–356.

Jiang, N., 2006. Hydrothermal alteration of chevkinte–(Ce) in the Shuiquangou syenitic intrusion, northern China. Chemical Geology 227, 100–112.

Kartashov, P.M., Ferraris, G., Ivaldi, G., Sokolova, E., McCammon, C.A., 2002. Ferriallanite–(Ce), $CaCeFe^{3+}$ $AlFe^{2+}$ $(SiO_4)(Si_2O_7)$

O(OH), a new member of the epidote group: description, X-ray and Mössbauer study. Canadian Mineralogist 40, 1641–1648.
Kaul, P.F.T., Cordani, U.G., 2000. Geochemistry of the Serra do Mar (southern Brazil) granitoid magmatism and tectonic implications. Revista Brasileira de Geociências 30, 115–119.
King, P.L., White, A.J.R., Chappel, B.W., Allen, C.M., 1997. Characterizations and origin of aluminous A-type granites from the Lachlan Fold Belt, Southeastern Australia. Journal of Petrology 38, 371–391.
King, P.L., Chappell, B.W., Allen, C.M., White, J.R., 2001. Are A-type granites the high-temperature felsic granites? Evidence from fractionated granites of the Wangrah Suite. Australian Journal of Earth Sciences 48, 501–514.
Lameyre, J., Bowden, P., 1982. Plutonic rock type series: discrimination of various granitoid series and related rocks. Journal of Volcanology and Geothermal Research 14, 169–189.
Liégeois, J-P., 1998. Preface — some words on the post-collisional magmatism. Lithos 45, xv–xvii.
MacDonald, R., Belkin, H.E., 2002. Compositional variation in minerals of the chevkinite group. Mineralogical Magazine 66, 1075–1098.
MacDonald, R., Marshall, A.S., Dawson, J.B., Hinton, R.W., Hill, P.G., 2002. Chevkinite-group minerals from salic volcanic rocks of the East African Rift. Mineralogical Magazine 66, 287–299.
McDowell, S.D., 1979. Chevkinite from the Little Chief Granite porphyry stock, California. American Mineralogist 64, 721–727.
Michael, P.J., 1984. Chemical differentiation of the Cordillera Paine granite (southern Chile) by *in situ* fractional crystallization. Contributions to Mineralogy and Petrology 87, 179–195.
Novak, S.W., Mahood, G.A., 1986. Rise and fall of a basalt–trachyte–rhyolite magma system at the Kane Springs Wash caldera, Nevada. Journal of Geophysical Research 94, 352–373.
Noyes, H.J., Wones, D.R., Frey, F.A., 1983. A tale of two plutons: petrographic and mineralogical constrains on the petrogenesis of the Red Lake and Eagle Peak plutons, Central Sierra Nevada, California. Journal of Geology 91, 353–379.
Parodi, G.C., Della Ventura, G., Mottana, A., Raudsepp, M., 1994. Zr-rich non metamictic perrierite–(Ce) from holocrystalline ejecta in the Sabatini volcanic complex (Latium, Italy). Mineralogical Magazine 58, 607–613.
Pearce, J.A., Harris, N.B.W., Tindle, A.G., 1984. Trace element discrimination diagrams for the tectonic interpretation of granitic rocks. Journal of Petrology 25, 956–983.
Petrík, I., Broska, I., Lipka, J., Siman, P., 1995. Granitoid allanite–(Ce); substitution relations, redox conditions and REE distributions (on an example of I-type granitoids, Western Carpathians, Slovakia). Geologica Carpathica 46, 79–94.
Pitcher, W.S., 1993. The Nature and Origin of Granite. Blackie Academic and Professional, England, pp. 218–237.
Platt, R.G., Wall, F., Williams, C.T., Woolley, A.R., 1987. Zirconolite, chevkinite and other rare earth minerals from nepheline syenites and peralkaline granites and syenites of the Chilwa Alkaline Province, Malawi. Mineralogical Magazine 51, 253–263.
Poitrasson, F., 2002. In situ investigations of allanite hydrothermal alteration: examples from calc-alkaline and anorogenic granites of Corsica (southeast France). Contributions to Mineralogy and Petrology 142, 485–500.
Robinson, D.M., Miller, C.F., 1999. Record of magma chambers processes preserved in accessory mineral assemblages, Aztec Wash pluton, Nevada. American Mineralogist 84, 1346–1353.
Scaillet, D., MacDonald, R., 2001. Phase relations of peralkaline silicic magmas and petrogenetic implications. Journal of Petrology 42, 825–845.
Segalstad, T.V., Larsen, A.O., 1978. Chevkinite and perrierite from the Oslo region, Norway. American Mineralogist 63, 499–505.
Siga Jr., O., Basei, M.A.S., Machiavelli, A., 1993. Evolução geotectônica da porção NE de Santa Catarina e SE do Paraná, com base em interpretações geocronológicas. Revista Brasileira de Geociências 23, 215–223.
Sommer, C.A., Lima, E.F., Nardi, L.V.S., Liz, J.D., Waichel, B.L., 2006. The evolution of Neoproterozoic magmatism in Southernmost Brazil: shoshonitic, high-K tholeiitic and silica-saturated, sodic alkaline volcanism in post-collisional basins. Anais da Academia Brasileira de Ciências 78, 573–589.
Speer, J.A., 1987. Evolution of magmatic assemblages in granitoid rocks: the hornblende+melt=biotite reaction in the Liberty Hill pluton, South Carolina. American Mineralogist 72, 863–878.
Troll, V.R., Sachs, P.M., Schmincke, H.-U., Sumita, M., 2003. The REE-Ti mineral chevkinite in comenditic magmas from Gran Canaria, Spain: a SYXRF-probe study. Contributions to Mineralogy and Petrology 145, 730–741.
Van Bergen, M.J., 1984. Perrierite in siliceous lavas from Mt Amiata, central Italy. Mineralogical Magazine 48, 553–556.
Vazquez, J.A., Manning, C.E., Reid, M.R., 2004. Experimental determination of allanite stability in high-silica rhyolite. Eos Transactions of AGU, 85, Fall Meeting Supplement, Abstract V41C-1407.
Vilalva, F.C.J., 2004. Evolução textural e do quimismo de minerais em granitos de tipo A: Comparação entre as associações aluminosa e alcalina do Maciço Morro Redondo, PR-SC. Monografia de Trabalho de Formatura. Universidade de São Paulo. 47 pp.
Vilalva, F.C.J., Vlach, S.R.F., 2006. Petrography and mineralogy of the peralkaline granites from the Morro Redondo Complex (PR-SC), south Brazil, and some constraints for the development of rare minerals. Workshop on A-type Granites and Related Rocks Through Time (IGPC 510). Belém, Brazil, p. 76.
Vlach, S.R.F., Janasi, V.A., Vasconcellos, A.C.B.C., 1990. Associated calc-alkaline and aluminous A-type late Brasiliano granitoids in the States of São Paulo and Paraná, southern Brazil. Annals of the XXXVI Brazilian Congress of Geology, vol. 4. Natal, Brazil, pp. 1700–1711.
Vlach, S.R.F., Janasi, V.A., Vasconcellos, A.C.B.C., 1991. O magmatismo granitóide tardi-a pós-orogênico de idade brasiliana no Estado de São Paulo. Boletim do IGc-USP, Publicação Especial, vol. 9, pp. 99–101.
Vlach, S.R.F., Siga Jr., O., Gualda, G.A.R., Basei, M.A.S., Hyppolito, T., Vilalva, F.C.J., 2006. Precise zircon U–Pb (TIMS) dating of dioritic rocks and implications for the age of the Graciosa Province of A-type granites and syenites, southern Brazil. Workshop on A-type Granites and Related Rocks Through Time (IGPC 510). Belém, Brazil, p. 77.
Watson, E.B., Harrison, T.M., 1983. Zircon saturation revisited: temperature and composition effects in a variety of magma types. Earth and Planetary Science Letters 64, 295–304.
Whalen, J.B., Currie, K.L., Chappell, B.W., 1987. A-type granites — geochemical characteristics, discrimination and petrogenesis. Contributions to Mineralogy and Petrology 95, 407–419.
Wones, D.R., 1989. Significance of the assemblage titanite+magnetite+quartz in granitic rocks. American Mineralogist 74, 744–749.
Wood, S.A., Ricketts, A., 2000. Allanite–(Ce) from the Eocene Casto granite, Idaho: response to hydrothermal alteration. Canadian Mineralogist 38, 81–100.
Yang, Z., Fleck, M., Smith, M., Tao, K., Song, R., Zhang, P., 2002. The crystal structure of natural Fe-rich chevkinite–(Ce). European Journal of Mineralogy 14, 969–975.